THESIS FOR THE DEGREE OF LICENTIATE OF ENGINEERING

Vehicle emissions abatement: NO oxidation and ammonia SCR

XAVIER AUVRAY

CHALMERS

Chemical Engineering
Department of Chemical and Biological Engineering
CHALMERS UNIVERSITY OF TECHNOLOGY
Göteborg, Sweden 2011

Vehicle emissions abatement: NO oxidation and ammonia SCR
Xavier Auvray

Licentiatuppsatser vid Institutionen för kemi- och bioteknik
Chalmers tekniska högskola
Serie nr. 2011:17
ISSN: 1652-943X

Department of Chemical and Biological Engineering
Competence Centre for Catalysis
Chalmers University of Technology
SE-412 96 Göteborg
Sweden
Telephone +46 (0)31 772 1000

Chalmers Reproservice
Göteborg, Sweden 2011

Vehicle emissions abatement: NO oxidation and ammonia SCR

XAVIER AUVRAY
Department of Chemical and Biological Engineering
Chalmers University of Technology, 2011

Abstract:

The design and the development of catalytic systems for reducing vehicle emissions is a complex task due to the variety of components in a wide range of gas flow and temperature. A complete system is, therefore, composed of a series of catalysts or catalytic systems, each of which is dealing with a particular aspect of the abatement process. A Diesel Oxidation Catalyst (DOC) is used for CO and hydrocarbon oxidation as well as the conversion of NO to NO_2. The NO_2 is used by the downstream processes, i.e. Diesel particulate filter (DPF) and NO_x reduction catalyst. In the DPF the particulates are removed and the regeneration of the DPF is enhanced by the presence of NO_2. One promising technique to remove the nitrogen oxides are urea selective catalytic reduction (SCR). Urea is decomposed to form ammonia, which reacts selectively with NO_x over a catalyst. The SCR rate increases with 50% NO_2 to NO_x ratio, which again shows the importance of the NO oxidation process.

In the first study, a model Pt-based DOC was studied for NO oxidation. The effect of ageing in various conditions was examined. More specifically, the impact of the ageing on the NO oxidation activity and platinum dispersion was investigated. Thermal aging caused a decrease in dispersion and an increase in NO oxidation performance. However, the ageing behavior was strongly correlated with the nature of the ageing atmosphere. It was found that ageing at low temperatures in O_2 promotes the activity to a greater extent than after aging in Ar, even though the dispersions are similar for the two samples. Ageing in SO_2 and O_2 led to a rapid dispersion drop to a minimum value and tremendously enhanced the activity. A long-term ageing in presence of SO_2 at 250°C confirmed the ability of SO_2 to increase sintering rate and improved catalyst activity. The results clearly show that NO oxidation activity is controlled both by the dispersion as well as the atmosphere the platinum particles were aged in. The combination of SO_2 and O_2 during aging resulted in the highest NO oxidation activity.

In the second study that was focused on NH_3-Selective Catalytic Reduction, intra-catalyst measurements of reaction and NH_3 storage were performed using a unique tool: the SpaciMS. The spatial conversions at three temperatures (200, 325 and 400°C) were resolved showing a faster reaction at higher temperature. The same trend was observed for the direct oxidation of NO and NH_3.The fraction of the catalyst, used to carry out the reaction until full conversion of NH_3, was named “SCR zone” and became smaller at higher temperature and a higher reaction rate. During SCR, NH_3 could store on the catalyst until complete saturation of the SCR zone. Surface NH_3 was able to react with NO in the gas flow according to SCR reaction equation yielding production of N_2 and the formation of a small amount of N_2O. NH_3 storage capacity during SCR (DC) was compared to the total NH_3 storage capacity (TC). In the SCR zone, DC followed TC and no significant unused capacity (UC) was observed, indicating that, in the presence of NH_3, storage sites are filled even during SCR operation in the SCR zone.

List of publications:

Spatiotemporal analysis of transient ammonia SCR experiments over Cu-Beta
Submitted

The effect of gas composition during thermal aging on the dispersion and NO oxidation activity over a Pt/Al_2O_3 catalyst
Manuscript

Contribution to the papers:

Paper I:
I performed the experiments, analyzed the results together with my co-authors and wrote the first manuscript.

Paper II:
I synthesized the catalysts and conducted the experiments. I interpreted the results with my co-author and wrote the manuscript.

Contents

List of abbreviations

TWC	Three-way catalyst
LNT	Lean NO_X-trap
NO_X	nitrogen oxides
SCR	Selective Catalytic Reduction
HC	Hydrocarbon
DOC	Diesel Oxidation Catalyst
DPF	Diesel Particulate Filter
DFT	Density Functional Theory
TPD	Temperature Programmed Desorption
TOR	Turn Over Rate
XPS	X-ray Photoelectron Spectroscopy
TPR	Temperature Programmed Reduction
PSD	Particle Size Distribution
EXAFS	Extended X-ray Absorption Fine Structure
BET	Brunauer Emmett Teller
SpaciMS	Spatially-resolved Capillary Inlet Mass Spectrometer
FTIR	Fourier Transform Infrared
CFD	Computational Fluid Dynamics
ORNL	Oak Ridge National Laboratory
MS	Mass Spectrometer
PM	Particulate Matter
DC	Dynamic Capacity
UC	Unused Capacity
TC	Total Capacity

1. Introduction

The emission of CO_2 which is a greenhouse gas and the consumption of fossil fuels are two environmental and economical issues nowadays. Greenhouse gas emissions and fuel consumption are targeted. Since the transportation sector represents a large part of global carbon dioxide emissions as well as global fuel consumption, a great effort has been devoted to develop more fuel-efficient engines like Diesel and lean-burn gasoline engines. For a more complete reaction, these engines work at higher air/fuel ratio which has a beneficial effect on fuel economy and also reduces carbon dioxide release. As a consequence, the nature of the exhaust gas is also modified and is now globally oxidizing to due to excess oxygen in the engine feed. This characteristic has a big impact on the catalytic treatment of the exhaust. After the introduction of emission regulation in the USA (TIER) and in Europe (EURO) in the 70's, catalytic systems were developed to reduce the emission of three types of harmful compounds: hydrocarbons (HC), carbon monoxide (CO) and NO_x, i.e. NO and NO_2. The catalyst used so far in gasoline engines, called three-way catalyst (TWC), could oxidize HC and CO into CO_2 and H_2O and, at the same time, reduce NO_x in H_2O and N_2. Unfortunately, as shown in Figure 1, TWC can only work within a narrow of air/fuel ratio window centered around 14,6. Diesel and lean-burn engines operate off this critical window and TWC can oxidize HC and CO but cannot handle NO_x in these oxidizing conditions.

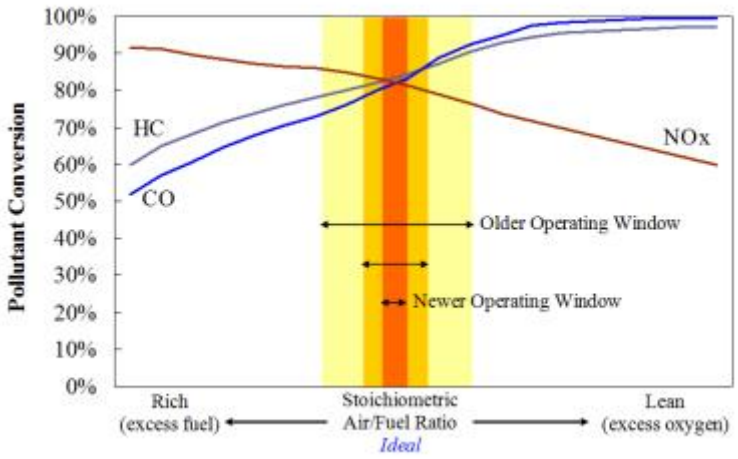

Figure 1: Operating window of TWC for HC and CO oxidation and NO_x reduction (*source: Environex Inc.*).

The release of NO_x in the atmosphere has disastrous consequences on urban air quality with the formation of ground-level ozone and of brown haze called "smog" which can provoke respiratory problems such as asthma due to its irritant properties. NO_x are also able to react with water to form nitric acid yielding acid rains. Therefore, more restrictive emission regulations have been introduced and forced the design of new catalytic systems to reduce NO_x produced by Diesel and lean-burn vehicles. Two processes aiming to reduce vehicle NO_x emissions have emerged in the 90's.

The lean NO_x-trap (LNT) technique is based on cycling the operating regime of the engine between fuel-lean and fuel-rich. During the lean period, NO_x are stored on the catalyst designed

to trap NO_x in form of surface nitrates thanks to an alkaline metal like barium. When the catalyst cannot trap sufficient amount of the NO_x, the regime is switched to rich mode by increasing the ratio of fuel/oxygen for a few seconds. Thus the excess of unburned fuel in the exhaust is used as a reductant to convert stored NO_x into N_2 and H_2O. This technique requires a very precise control of the engine and the catalyst and the rich periods penalize the fuel economy.

The second method consists of the selective catalytic reduction (SCR) of NO_x by injecting a reductant in the gas stream upfront the catalyst. The mixture containing NO_x and the reducing agent traverses a catalyst upon which the reduction of NO_x into N_2 and H_2O occurs. Many types of catalysts and reductants have been studied. The fuel can be used as a source of hydrocarbons for HC-SCR, which led to many studies [1, 2]. NH_3 is able to reduce selectively NO and can be produced in situ by the decomposition of a urea solution. NH_3-SCR does not involve direct extra fuel consumption but demands a tank to store the urea onboard as well as an accurate dosing system.

In exhaust gases, NO_x is mainly composed of NO and yet the two aforementioned processes are more efficient when treating a NO_2-enriched gas stream. Indeed NO oxidation in NO_2 has been demonstrated to be the first step of the LNT process and the activity of NH_3-SCR is greatly enhanced by the presence of NO_2 up to a NO_2/NO of 1. The catalytic system of a Diesel vehicle then contains a catalyst devoted to oxidation of NO placed upstream of the NO_x reduction catalyst to make the NO_x conversion faster. NO_2 is a powerful oxidant and, as a consequence, NO_2 produced by the Diesel oxidation catalyst (DOC) is utilized for the regeneration of Diesel particulate filters (DPF), another catalytic process devoted to the capture of the soot particles emitted by Diesel engines. Finally DOC's second task is to oxidize CO, gaseous HC and liquid HC responsible for the emission of particulate matters. Figure 2 shows a complete exhaust treatment system combining DOC, DPF and NH_3-SCR catalyst.

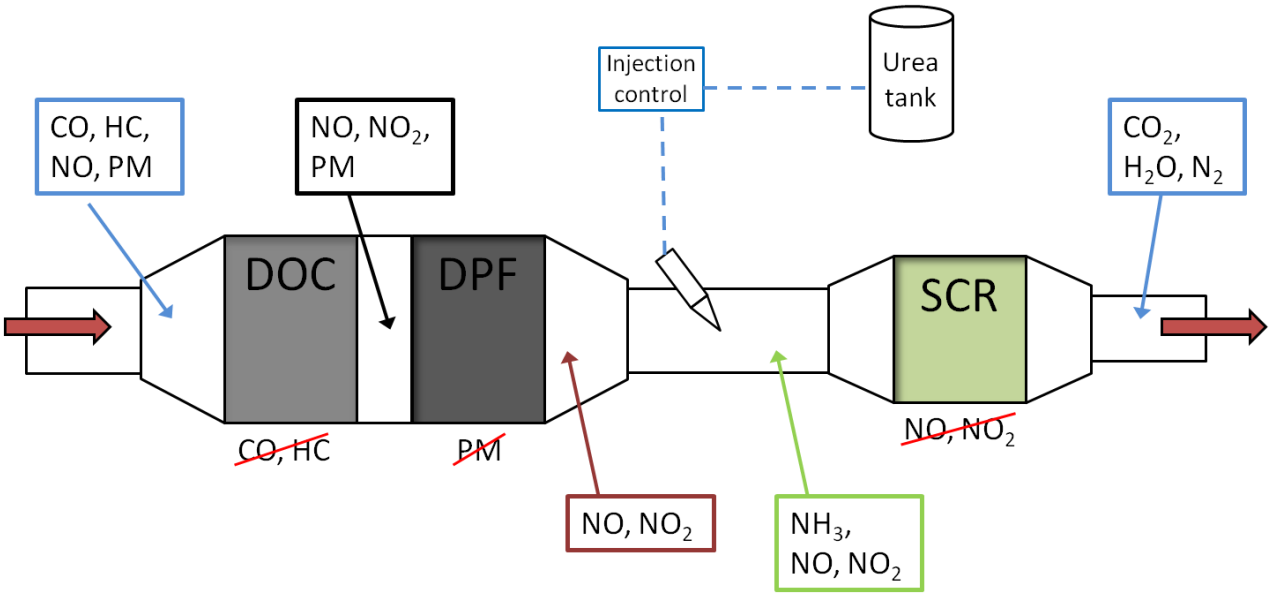

Figure 2: Combination of catalysts to reduce emissions of Diesel vehicles.

2. Objective

The purpose of the first study is to investigate the effect of ageing under a reactive atmosphere of a Pt-based Diesel oxidation catalyst. To understand the ageing occurring during the lifetime of a catalyst, ageing conditions were reproduced and applied to a Pt/Al_2O_3 catalyst. The specific effect of the gas composition on the sintering and further activity of the catalyst is shown with a focus on NO oxidation.

The second study is focused on the selective catalytic reduction of NO by ammonia on a copper exchanged beta zeolite. SpaciMS was used to reveal intra-catalyst partition of various phenomena like NH_3 storage, reactants consumption and the formation of products under different operating conditions. Transient and steady state behaviors are studied at 200, 325 and 400°C, respectively.

3. Bibliographic study

3.1. NH_3-SCR

The selective catalytic reduction (SCR) is a method of NO_x reduction which involves the direct reaction of NO_x with a reductant over the catalyst. It necessitates the injection of an additional reductant into the exhaust gas stream or the catalytic production from the exhaust of a reducing agent like H_2 or CO. This technique is already efficiently employed on stationary NO_x sources like boilers and power plants but its adaptability to mobile and regime-changing sources like vehicles remains a challenge. The time adjustment of the amount of reductant injected becomes tricky due to the variations in temperature and engine workload. The next section focuses on the SCR performed with NH_3 as reductant.

The reduction of NO_x with ammonia has proved to be efficient when applied to stationary sources and does not require extra fuel to reduce NO_x, unlike NSR and hydrocarbon-SCR. On the other hand, ammonia must be stored and carried onboard in an additional tank which is also constraining the application on passenger cars but acceptable for heavy-duty trucks.

The reaction equation in oxygen-containing conditions involves as much NO as NH_3 and gives N_2 and H_2O (1)

$$4NO + 4\,NH_3 + 3O_2 \rightarrow 4N_2 + 6H_2O \quad (1)$$

The reaction (1) is often referred to standard SCR and takes place when the NO content of NO_x is 100%. The fraction of NO in real exhausts is not 100%, though since NO_2 is also emitted by Diesel and lean-burn engines which triggered the investigations into the reduction of NO_2 and a mixture of both NO and NO_2 according to the two following equations:

$$4NH_3 + 2NO + 2NO_2 \rightarrow 4N_2 + H_2O \quad (2)$$

$$4NH_3 + 3NO_2 \rightarrow \frac{7}{2}N_2 + 6H_2O \quad (3)$$

Reaction (2) is called fast-SCR because it occurs faster than the standard SCR and shows a maximum rate with equal amounts of NO and NO_2 [3-6]. The relative rate of the third reaction depends on the catalyst and the conditions under which it is used. The NO_2 SCR can be faster than the standard SCR on a Fe-zeolite catalyst [7] but slower on a vanadia-based catalyst [4]. In general, the rate of reaction of SCR increases with concentrations of O_2 and NO_x but NH_3 inhibits the reaction by blocking the active sites for NO adsorption and oxidation [7].

3.1.1. Catalysts

Commercial catalysts based on vanadium oxide, like V_2O_5-WO_3/TiO_2, have been extensively studied for their excellent activity and selectivity [4, 5] for ammonia SCR. Their major drawbacks are the volatility and toxicity of vanadium oxide and a lack of efficiency at low and high temperatures. The ideal catalyst for an automotive application would cover a wide range of temperature since it is low for few minutes after starting the engine and high when a particle filter placed upstream is regenerating. Ion-exchanged zeolite catalysts have also been investigated more recently [3, 8-10] because they do not contain precious metal and are

consequently less expensive. Iron and copper ion-exchanged zeolites have been especially well-regarded and have evidenced a good ability to reduce NO_x but their deactivation after hydrothermal ageing must be improved.

3.1.2. Side reactions

In general, several reactions other than SCR involving either NO or NH_3 occur on the catalyst. These reactions have a detrimental impact on the selectivity and on the catalyst efficiency because their product is not N_2 and because they lead to overconsumption of NH_3, respectively.

At low temperature (<200°C), the main side reaction is the formation of ammonium nitrate [4, 5, 8] onto the catalyst (see reaction (4)). NH_4NO_3 can form a deposit on the catalyst or sublimate to exit the catalyst in the gas flow.

$$2NH_3 + 2NO_2 \rightarrow NH_4NO_3 + N_2 + H_2O \quad (4)$$

The NH_4NO_3 can subsequently react. According to Koebel et al. [4], it decomposes in NH_3 and nitric acid to oxidize NO to NO_2 which enhances the SCR reaction. In that case, ammonium nitrate is an intermediate species that builds up in presence of NO_2 and then decomposes according to the SCR reaction. The decomposition in N_2O and water (eq. 5) is another possible problematic alternative since it affects directly the selectivity.

$$NH_4NO_3 \rightarrow N_2O + 2H_2O \quad (5)$$

The second undesirable reaction is the formation of N_2O which decreases the selectivity. It is attributed to the direct oxidation of NH_3 according to the following reaction (6).

$$4NH_3 + 4O_2 \rightarrow 2N_2O + 6H_2O \quad (6)$$

This route is the major source of N_2O over vanadia-based catalysts. Since NO_2 is a stronger oxidant than O_2, it also participates in the oxidation of NH_3 too. This reaction was found to be predominant over Fe-zeolite SCR catalyst by Devadas et al. [3] whereas no N_2O was formed when only NH_3 and O_2 flowed through the catalyst suggesting that the direct NH_3 oxidation (reaction (6)) is not responsible for N_2O production on this type of catalyst. At high temperature, N_2O decomposes in N_2 and O_2 and can also be reduced in parallel by NH_3 yielding an overconsumption of NH_3. With intra-catalyst measurements, Luo et al. showed that N_2O builds up in the front part of Fe/zeolite catalysts and that a fraction subsequently decomposes in the rear part of the catalyst at 500°C [7]. At low temperature N_2O generation can be explained by the decomposition of ammonium nitrate as previously mentioned (reaction (5)).

At high temperature, direct oxidation of ammonia is observed leading to an overconsumption of NH_3. This reaction lowers the NO_x reduction due to the competition for ammonia. It has been observed over Cu-ZSM-5 that this reaction starts from 200°C when only NH_3 and O_2 are in the gas flow and the decrease of SCR observed at higher temperature can be ascribed to ammonia oxidation [9, 11]. Moreover the product of ammonia oxidation observed was N_2 [9]and not NO suggesting the following reaction equation:

$$4NH_3 + 3O_2 \rightarrow 2N_2 + 6H_2O \quad (7)$$

Cu-exchanged zeolite catalysts showed a high level of activity for SCR with ammonia and also limit side reactions. The NH_3 conversion and the NO conversion were found to be equal up to around 600K, indicating a NH_3/NO stoichiometry of 1 and negligible side reactions [9, 11]. At higher temperature, NH_3 starts to be oxidized by O_2.

To summarize, NO_2 enhances the NH_3 SCR but is also responsible for NH_3 oxidation, NH_4NO_3 formation over vanadia-based catalyst and N_2O generation over metal-exchange zeolite depending on the temperature. Thus, the NO_2/NO_x ratio should be well adjusted and, for optimal operation of the NO_x emission control catalytic system, it should not exceed 0,5.

3.2. NO oxidation

The oxidation of NO to NO_2 is a crucial reaction involved in both NO_x-removal processes. It is indeed considered to be the first step of NO storage on NSR catalysts and increases the NO_2/NO ratio of the gas mixture, thereby enhancing the activity of SCR catalysts. Since NO_2 is a powerful oxidant, the oxidation of NO is a good way to produce in situ NO_2 in order to regenerate DPF (Diesel Particulate Filter) by burning the trapped soot. This reaction is performed on common oxidation catalysts such as Pt-based catalysts.

3.2.1. Kinetics and thermodynamics

The conversion of NO is limited by the activation energy at low temperature and by the thermodynamic equilibrium at high temperature. To ameliorate the performance of such catalysts, the activity at low temperature needs to be improved.
The reaction follows the equation:

$$NO + ½\ O_2 \rightarrow NO_2 \qquad \Delta G° = -35348\ J/mol$$

The actual catalytic reaction is considered to occur step by step according to the Langmuir-Hinshelwood mechanism depicted in Figure 3.

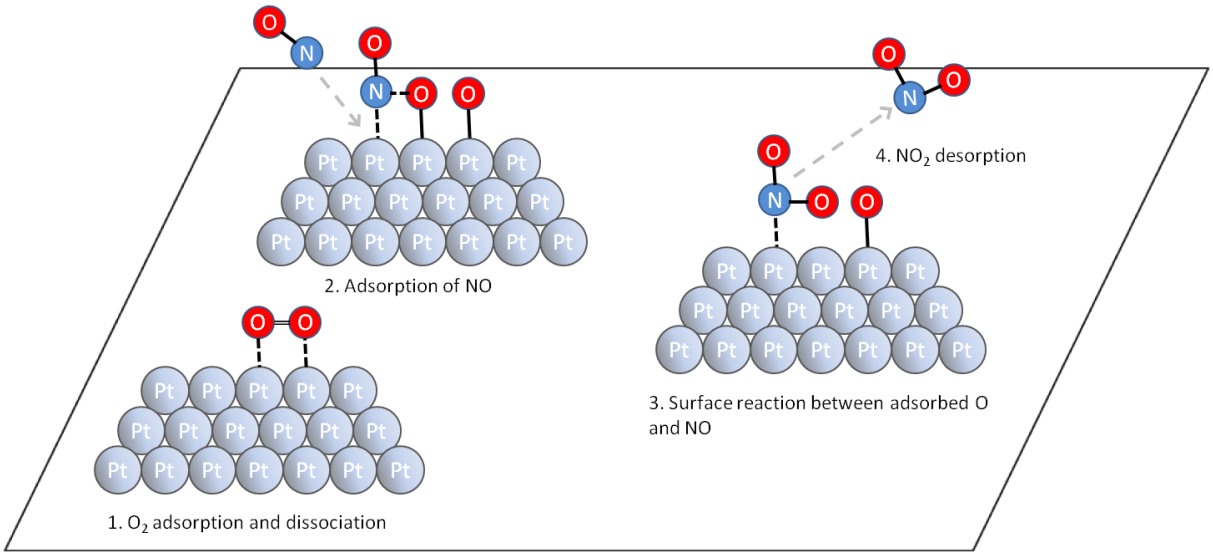

Figure 3: Catalytic oxidation of NO according to Langmuir-Hinshelwood mechanism.

The reaction is exothermic with a standard $\Delta H_f° = -57{,}19$ kJ/mol. The concentrations of the reactants affect the performance of the catalyst. Thus, on Pt/SiO_2, the conversion is higher when the NO concentration is lower [12, 13]. The opposite effect of O_2 is observed and the increase of its fraction up to 20% of the gas flow enhances significantly the overall conversion and oxidation rate [12]. NO_2, as the product of reaction, has a negative impact and causes deactivation of the catalyst by forming persistent platinum oxide.

In their model, Olsson et al. [14] reported an activation energy of 40,8 kJ/mol for NO oxidation. Similar results were found elsewhere [15-17]. Mulla et al. [16] took into account the presence of NO_2 in their kinetic model of NO oxidation over Pt/Al_2O_3 and showed that the activation energy became twice as it was without NO, i.e. ca. 80 kJ/mol, confirmed by the results of Smeltz et al.

[18] and Bhatia et al. [19]. In the following study, Mulla et al. also found a positive first order in both O_2 and NO and negative first order in NO_2 and they reported a decreasing of reaction order for O_2 for sintered Pt/Al_2O_3 catalyst to approximately 0,7[20]. The rate determining step has been identified by density functional theory (DFT) [21] and global kinetic modeling [19] as the adsorption/desorption of O_2 in the Langmuir-Hinshelwood model.

3.2.2. Effect of the support

Many catalysts containing metal have been tested and modeled and platinum appeared to be a good candidate for further studies [12, 15, 17, 19, 20]. Thus, the activity of platinum has been measured for a range of metal oxide supports and platinum loadings [17, 22, 23]. The supports may be classified, based upon the conversion obtained, in the following order SiO_2>γ-$Al2O_3$>CeO_2>TiO_2>ZrO_2 [22, 23]. The specific surface area of the support is an important factor but the Pt-support chemical interaction is also a crucial parameter in the activity of the catalyst.

The storage of NO_x on the support influences the rate of reaction. Benard et al. [23] assumed that the good performance of SiO_2 was due to the weak bonds formed between NO_2 and NO and this support according to NO-TPD experiments. Thus, NO is weakly adsorbed on SiO_2 and migrates readily to Pt atoms in order to be oxidized. Xue et al. also found that SiO_2 adsorb very little NO_x while Pt/SiO_2 catalysts showed a broad peak of NO desorption and concluded that the contribution of SiO_2 on the storage of NO was negligible compared to the adsorption on Pt sites [22].

The situation is different when the support is alumina on which Xue et al. [22] observed a stronger adsorption of NO and NO_2 than on SiO_2. The TPD of NO and NO_2 on Pt/Al_2O_3 and bare Al_2O_3 resulted in that a bigger quantity of NO desorbed from Al_2O_3 than from Pt/Al_2O_3. As Al_2O_3, ZrO_2 has a good ability for adsorbing NO and NO_2.

The difference between the supports originates from their acido-basic properties. SiO_2 is acidic and does not form strong bond with acidic molecules such as NO, NO_2 or SO_2 while Al_2O_3 is amphoteric with the consequence that aluminum nitrates, nitrites or sulfates are easily formed on its surface.

3.2.3. Effect of the particle size

When a catalyzed reaction has a rate which changes with the morphology of the catalytic agent, it is called structure sensitive. NO oxidation over Pt-based catalysts is one of those reactions. Indeed, studies that correlate the activity to particle size or platinum dispersion are numerous [17, 20, 22, 24] and show that the reaction is quick when it occurs on the surface of big particles whereas the rate observed for small particles is low. Clayton et al. reported a maximum activity for particles of intermediate size [25] but the activity curves of their catalysts do not superpose at high temperature suggesting that they do not reach thermodynamic equilibrium. Mulla et al. evidenced the structure sensitivity of the reaction by calculating the Turn-Over Rate (TOR) of fresh catalysts, with small particles, and sintered catalysts, with big particles [20]. The TOR is defined by the number of molecules of NO oxidized per surface atom of platinum per time which yields an intensive measure of the rate of a catalytic reaction. The TOR reported for the sintered catalyst was higher than the TOR of the fresh catalyst which confirmed that big particles are more active than small particles.

This property is surprising since sintering yields loss of active sites and, consequently the deactivation of the catalyst. However, this effect is largely compensated by the better activity of resulting larger particles. In their global model for CO oxidation, Yang et al. [26] demonstrated that bigger particles had a superior intrinsic activity than smaller ones due to a kinetic constant assumed higher for atoms on a plane than for corner and edge atoms (k_{plan}/k_{other}=2,5). But for this reaction, contrary to NO oxidation, the increased performance of the particles does not compensate for the loss of active sites. The impact of the dispersion varies for different supports and is more pronounced on Pt/SiO_2 than on Pt/Al_2O_3. However, the reaction does not seem size dependent on Pt/ZrO_2 [22].

The reason evoked in the literature to explain the incredible activity of big particles is their better resistance towards oxide formation by weakening the O-Pt bond [20, 23]. Indeed, many studies attributed the deactivation of the oxidation catalyst to the formation of platinum oxide, as discussed in the next section. Numerous reactions are affected by this deactivation, such as NO oxidation [20, 24] and the combustion of propane [27].

3.2.4. Effect of the oxygen coverage

In homogeneous catalysis, the interactions of the active metal and both reactants and products are fundamental. A catalyst must be able to form bonds of a well-dosed strength with reactants. When the bond is too weak, the coverage will be too low to react quicker. Moreover, it will be difficult to dissociate molecules like O_2 or N_2. On the other hand, if the interaction is too strong, the molecule cannot diffuse at the surface and pair with second adsorbed species to react. Another consequence of strong bonds is the blocking of active sites by adsorbed molecules which hinders the reaction and poisons the catalyst. The issue is analogous to the product which must be easily released by the catalyst to avoid blocking sites and poisoning.

Depending on their size, platinum particles exhibit active sites with different properties regarding their interaction with oxygen. Many studies have been undertaken in order to characterize the oxygen-bonding with various types of Pt surfaces. Ovesson et al [28] included the oxygen coverage in their study of NO oxidation on Pt(111) facet and showed that the reaction is ignited by a minimum oxygen coverage which depends on the temperature; higher minimum coverage is required to start the reaction at lower temperature. Also the NO oxidation reaction has been found to be theoretically endothermic on this surface. However, thanks to lateral repulsive interactions between neighbor adsorbed oxygen atoms, it becomes exothermic and Pt(111) catalyses the reaction at high O-coverage. Mudiyanselage et al. [29] evidenced experimental results consistent with Ovesson's. They prepared covered-Pt(111) crystals via O_2 and NO_2 dissociative chemisorptions to obtain an O-coverage of 0,25 and 0,75 of the monolayer, respectively. Their TPD measurement revealed only one O_2 desorption peak centered at 700K for the low coverage crystal, while the high coverage crystal showed two additional releases at lower temperatures corresponding to weakly bonded oxygen atoms. NO_2 production was not observed on the sample with a coverage lower than 0,25ML, whereas NO_2 was formed easily even at room temperature on a highly covered surface which confirms that weakly bonded oxygen atoms are necessary for the reaction to proceed.

3.2.5. Deactivation of the catalyst

Loss of catalyst activity has been observed after long-term experiments [24] and was attributed by XPS analysis to platinum oxide formation which is thermodynamically favorable in actual reaction conditions. Indeed, platinum oxide reactivity has been evaluated by first principle calculations by Wang et al. [30] and compared with the metal form as well as other platinum group metal oxides. Unlike Os and Ir, the platinum oxide was found to be less active than its metal counterpart because the O_2 dissociation barrier is much larger on PtO_2 (110) (1,78eV) than on Pt (111) (0,49eV) [21]. The weak binding ability of PtO_2 (110) toward O, O_2 and NO is also pointed out as a reason for its low activity.

The passivating oxidation of platinum was studied by McCabe et al. [31] to elucidate the type of Pt oxides formed during exposure of the catalyst to O_2 at different temperatures and after ageing in various conditions. Chemisorbed oxygen, PtO and PtO_2 are the three species that can possibly form on the surface of platinum particles depending on the oxidation temperature and particle size. It was found that only surface atoms could be oxidized yielding a monolayer of passivating oxide specie. As a consequence, a larger amount of oxide is formed over highly dispersed catalysts. From TPR measurement, PtO_2 is assumed to be the dominant specie on the surface of small particles whereas the O:Pt stoichiometry of 1, found for bigger particles, do not allow us to state whether it implies formation of PtO or chemisorbed O. Since big particles are more readily reduced than small ones, the particle size plays a role in the reduction of the oxide.

NO_2 is a strong oxidant, the dissociation of which leads to the oxidation of the surface of Pt particles [16, 19]. This mechanism is believed to be the main cause of development of platinum oxide yielding catalyst deactivation.

3.3. Ageing of metal-based catalysts

3.3.1. Sintering mechanisms

High temperature treatment causes sintering of metallic crystallites, decrease of the dispersion and phase changes of the support [32]. The rate and extent of these phenomena are dependent on the conditions of ageing such as the temperature, the atmosphere composition and the duration of treatment.

Sintering increases with ageing temperature, as well as with ageing time. However the rate of sintering decays monotonically with time [33] until a dispersion limit corresponding to a stationary state is achieved [34]; the biggest change in particle size and dispersion occurs within a short time at the beginning of the ageing procedure [35]. Back in 1974, Flynn and Wanke [36-38]built a model to account for sintering and redispersion assuming that particle growth occurred via escape of atoms, or molecules like PtO, from small particles which migrate either on the surface or in the vapor phase to eventually integrate the structure of big particles (Figure 4). Their model is based on the rate of growth/shrinkage of the particles described by the following equation:

$$\frac{dN_i}{dt} = \alpha v \frac{F_s}{N_t S_0} D_i - A e^{-E_a/RT}$$

where
- α sticking probability of an atom colliding with a crystallite
- v velocity of atoms on the support
- N_t total metal atoms
- S_0 support area per metal atom
- F_s number of atoms migrating on support with an area N_tS_0 (i.e. F_s/N_tS_0 is the concentration of atoms on support surface)
- D_i effective diameter of the crystallite

is the number of atoms in the ith particle, $\alpha v \frac{F_s}{N_t S_0} D_i$ defines the number of atoms gained by the ith particle and the loss of atoms is given by the Arrhenius law for the extraction of a single atom $Ae^{-E_a/RT}$

The driving force of the sintering process is the reduction in surface energy during the transfer of atoms from small particles to bigger particles. In that model, also called Ostwald ripening, the size difference between particles may be considered as the driving force [36, 37]. As a consequence, the presence of one very large particle accelerates the sintering while no particle growth is observed when all particles have similar size. A broad particle size distribution (PSD) that indicates the presence of small and large particles on the same catalyst promotes the sintering via this mechanism.

The interaction of the support and the metal is fundamental to this model. A strong interaction will stabilize single atoms on the surface and lower the energy necessary for an atom to escape a particle. The presence of defects in the support structure is also a factor of localized energetic stabilization, as well as impurities on the surface. The effect of atmosphere is accounted for since the metal atom/support surface interaction can be modified by an atmosphere like O_2. At

an early stage of treatment, this model is in agreement with observed redispersion [39] since it expects an increase of atomic or molecular species on the support.

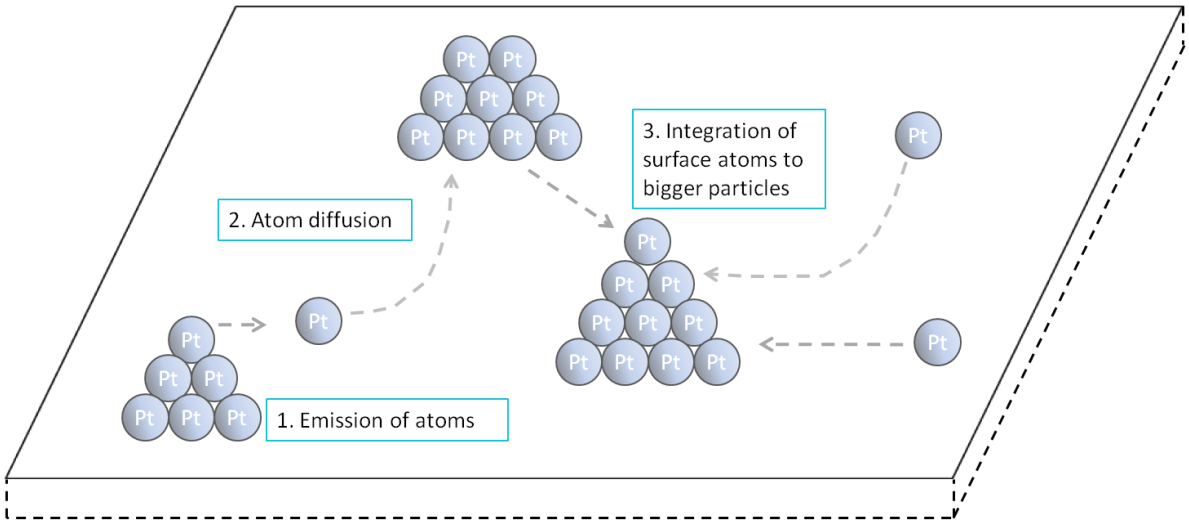

Figure 4: Ostwald ripening mechanism for particle sintering.

A second model based on the migration and coalescence of particles, without regard to their size, was proposed by Ruckenstein and Pulvermacher in 1973 [40] (Figure 5). The crystallites are considered mobile on the support and their collisions and fusion create bigger particles. It is, therefore, characterized by the shift of the particle size distribution towards larger size and the disappearance of small crystallites. The rate of decay of the metal surface was modeled by an empirical power law equation:

$$\frac{ds}{dt} = -Ks^n,$$

where *s* is the metal surface, K is the sintering rate constant and n is an integer.

This law suggests that, at any time, the size of every particle is supposed to be as large as or larger than the initial minimum particle size. The mobility of the particles is provided by the temperature or by the in situ production of gas like the evaporation of water [41]. It has then been modified to account for observed phenomena like the declining of the sintering rate with increasing particle diameter. Ruckenstein and Malhotra introduced the possibility of particle splitting to explain redispersion of metallic phase in their sintering model [42].

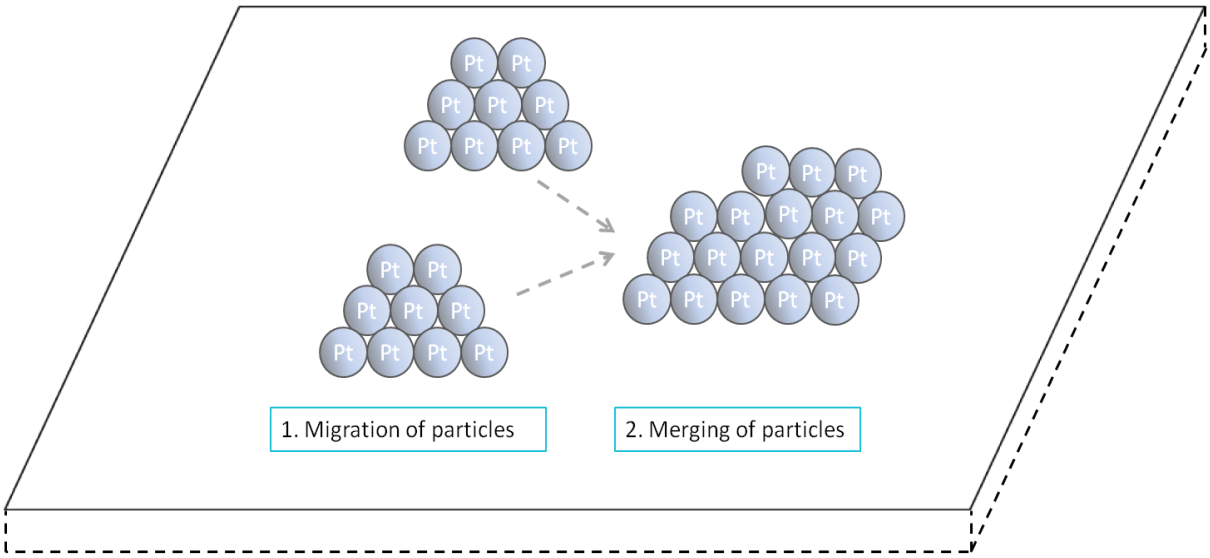

Figure 5: Illustration of the particle migration and coalescence model.

3.3.2. Effect of atmosphere on sintering rate of Pt catalyst

In the two sintering models, Particle Migration and Coalescence and Ostwald Ripening, particle-support interactions play an important role on mobility and stabilizing particles. During thermal treatment, metal particles create bonds with molecules in the atmosphere which changes the interactions between particles the support. Intermediate species, like metal oxide or metal complex, can be formed at the surface of the particles. These species have a lower temperature of vaporization than the corresponding metal and are, therefore, more likely to extract from the particle. It is, therefore, expected that an ageing atmosphere modifies the sintering rate through the formation and migration of mobile intermediate species. Contradictory effects of atmosphere on the sintering of Pt/Al_2O_3 are often found in the literature because of the differences between treatments such as temperature, Pt loading and exposure duration.

A reactive atmosphere can be classified in three categories: inert, reductive and oxidative. The effect of each varies with temperature and catalyst (support, loading, initial dispersion, etc…).

According to Lööf et al. [43], inert atmosphere such as Ar, a one-hour ageing at 700°C, does not cause sintering of platinum particles supported on alumina. However, they showed that a gas mixture containing H_2 induced a mild sintering starting at a threshold ageing temperature of 700°C. On a film model catalyst, however, Glassl et al. [35] observed that H_2 had a higher impact than O_2 and Ar on the sintering of Pt at low temperature (510K). A positive effect on sintering by H_2 has also been reported by Kamiuchi et al. at 200°C for a Pt/SnO_2 catalyst [44]. Accelerated of sintering in cycling oxidative and reductive conditions has been reported [32, 45]

To a larger extent, oxidative atmospheres enhanced the rate of particle growth [26]. Under oxidative conditions, this rate increased with ageing temperature. The maximum rate observed was for an atmosphere containing NO alone in Ar flowing over an oxidized catalyst. Such a mixture gave a high sintering rate at such a low temperature as 200°C. The oxidation of bulk platinum in platinum oxide lowers the energy of vaporization of Pt and increases the probability of atomic emission from particles. In that case, sintering according to the Ostwald ripening

mechanism seems to occur. Moreover, the PtO_x-Al_2O_3 bond is stronger than the metallic Pt-Al_2O_3 which makes the particles less mobile on the support and is against the migration and coalescence mechanism. However, evidence of sintering via the latter mentioned mechanism was observed when cycling reductive and oxidative treatment [32]. The oxidation of platinum and its subsequent reduction with H_2 forms water which then evaporates. This gas emission from the particles provides mechanical motion to the Pt particles as required by the sintering theory. A similar observation was made during the regeneration of coked catalyst in O_2 which produces CO_2 gas.

Other compounds present in exhaust gases in small quantities have been identified to cause sintering of platinum but have not yet been extensively investigated. Winkler et al. [46] showed that phosphorus poisons the catalyst by forming a contaminating layer around the particles. They also noticed that phosphorus led to larger particles indicating its implication in the sintering process. SO_2 is also an interesting compound and is believed to play a major role in sintering at low temperature, the effects of which will be discussed in detail in a later section.

3.3.3. Redispersion treatment

Unlike temperature, reactive atmosphere composition is an ageing parameter that does not only provoke sintering but can also lead to a partial redispersion of the metallic phase of a catalyst. Redispersion treatments have been perfected in order to reactivate aged industrial catalysts.

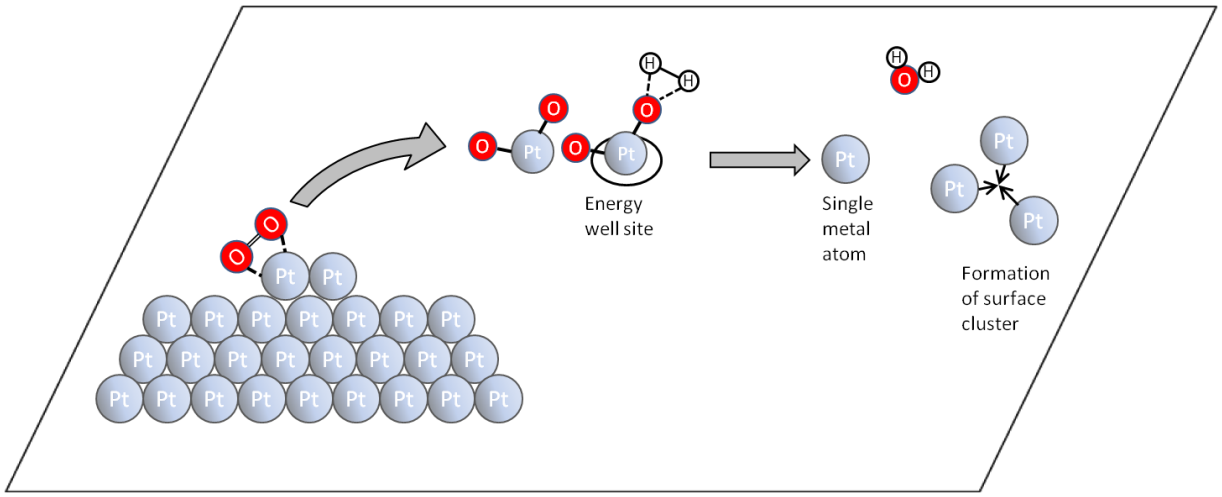

Figure 6: Schema of platinum redispersion in cycling oxidative/reducing conditions.

The principle of redispersion is to create intermediate species containing one metal atom or a cluster of metal atom which can readily extract from metal particle and migrate on the support to eventually deposit at another location. Treatment in oxidative atmosphere at a temperature between 500 and 600°C of sintered Pt/Al_2O_3 brings about the redispersion of platinum [38, 39, 47-49]. Treatment with chlorine, bromine or a combination of chlorine and oxygen is also efficient to increase the dispersion of deactivated catalysts [34, 39, 48]. A cycling oxidative-reducing treatment can yield redispersion as well [33, 50]. It has been proposed that, in an oxidative atmosphere, PtO_2 forms and migrates from big particles to the support. Since this oxide species become unstable at temperatures in the range of 550-600°C or in reducing conditions, they subsequently decompose to Pt and O_2 [47] (Figure 6). The presence of high

energy trapping sites on the support is also assumed to capture and maintain mobile Pt atoms or clusters on the surface before they collide with other particles and cause sintering. On a Pt-zeolite catalyst, Foger and Jaeger[51] showed that the redispersion with chlorine occurred via the formation of $PtCl_2$ crystals.

Other mechanisms were evoked like the splitting of particles [42] which can be implemented in the particle migration and coalescence model and the film formation [50, 52]. In the latter mechanism proposed by Ruckenstein[53], a metal film spreads from the particles over the support. In reducing atmosphere, the metal film breaks up into dispersed patches, which are believed to contract and give birth of new small particles.

3.4. Effect of SO_2

SO_2 is produced in small quantities as the result of the combustion of sulfur compounds contained in fuel and lubricants. Even in small concentrations, SO_2 can have important effects on an automotive catalyst and shorten its lifetime.

3.4.1. Deactivation

SO_2 is a Lewis base with one free pair of electrons which can bind to electrophile sites. Thus, SO_2 stores on automobile catalysts such as Pt/Al_2O_3. Summers showed that SO_2 adsorbs on bare Al_2O_3 and even ten times more SO_2 is adsorbed on Pt/Al_2O_3 in the absence of O_2 [54]. Xue et al. have also demonstrated the preferential adsorption of SO_2 on Pt rather than on alumina [22]. Introducing oxygen leads to an increase of sulfur storage enhanced by the oxidation of SO_2 in SO_3 which has a huge ability to store. The species formed over the surface are stable and decompose only at elevated temperature: desorption of SO_2 and SO_3 on alumina occurs at 600°C and beyond 800°C, respectively [55]. Consequently, sulfur adsorbates accumulate on the catalyst at normal operating temperature, covering the active sites and causing deactivation. Since it competes directly with NO_x storage and to form stable sulfates with the storage component, the storage of sulfur strongly affects the performance of NSR catalysts [55, 56]. The decrease of activity of commercial DOC catalysts and vehicle-aged catalysts after exposure to SO_2 indicates chemical poisoning caused by sulfur adsorption [57]. In this study, catalysts subject to a high SO_2 level and long-term exposure were severely deactivated.

Since a sudden fall of NO conversion is observed after introduction of SO_2 in the reaction feed, SO_2 inhibits NO oxidation [58, 59]. Pazmiño et al. showed no deterioration in activity after pre-adsorption of SO_2 [60] but revealed by XPS and EXAFS the presence of sulfur species on platinum after this pre-treatment. They proposed that adsorption of NO during the reaction displaced adsorbed SO_x to irrelevant sites since the Pt dispersion measurement after reaction suggested that surface Pt was not blocked by SO_x.

3.4.2. Promotion effect

Despite detrimental effects usually reported for SO_2, a beneficial effect has also been observed. Olsson and Karlsson [59] have noted a slow regaining of activity during their 22-hour experiment in SO_2-containing flow. They ascribed this result to the ability of SO_2 to promote platinum migration and sintering at low temperature (200 and 250°C). It is known that bigger Pt particles are more active for NO oxidation and therefore the promotion of Pt sintering yields increase of activity. The sintering of platinum was confirmed by the measure of dispersion before and after the experiment. Lee et al. [61] reported a promotion effect of SO_2 on the same type of catalyst (Pt/Al_2O_3) on propane oxidation which deactivates with the formation of Pt oxide. The amelioration observed was attributed to the reduction of PtO_2 and subsequent sintering of metal Pt caused by the presence of SO_2. Angelidis and Kruse [62] provided evidence of a promotional effect of SO_2 on HC-SCR of NO_x over Ag/Al_2O_3. Even though the light-off temperature increased in the presence of SO_2, the maximum conversion reached increased. SO_2 lowered the NO_2 production and hindered the storage of NO_x on silver. Furthermore, adsorbed species of the type RSO_x have also been identified suggesting, changes in the reaction mechanism.

4. Experimental part

4.1. Chemical and thermal ageing of a Diesel oxidation catalyst

4.1.1. Catalyst preparation and characterization

The Diesel oxidation catalyst prepared for the ageing study was a platinum-based catalyst supported on γ-Al_2O_3 containing 1% wt. of noble metal. It was synthesized by adding a solution of platinum nitrate to slurry of alumina dissolved in an ethanol solution. During the impregnation step, the pH of the solution was adjusted and maintained at 2, i.e. acidic conditions. Alumina is an amphoteric metal oxide which possesses surface hydroxyl groups, positively charged aqua groups, oxygen ions and incompletely unsaturated cations. These sites have electrical charges that can be controlled by the pH in the solution in the following manner: in acid medium the surface is most likely positively charged and $–(OH_2)^+$ groups are abundant. Inversely, the addition of a base produces a majority of negative oxygen ions. Surface groups play the important role of being anchor to the dissolved metal complex. Thus, if the Pt complex is anionic, as is the case in our synthesis, positively charged surface groups are desired and the impregnation must occur in acid solution. The mixture obtained was then freeze-dried to sublimate the water and then calcined 2h at 500°C to eliminate residual nitrates coming off the platinum precursor. A high dispersion of approximately 65% was achieved by using this method.

Monolithic coarses of cordierite were cut up, calcined 2h at 600°C and impregnated with a blend of powder containing 80% wt of the catalyst described above and 20% wt of a binder to optimize the grip of the washcoat on the channel walls. The Pt/Al_2O_3 powder was dissolved in a solution containing 50% wt. ethanol and 50% wt water. After soaking the monolith in the solution, drying and calcination were performed using a hot air gun at 600°C for 1min. The evaporation of the liquid phase was carried out thoroughly to deposit a uniformly thick layer of active phase throughout the monolith. The operation of impregnation and drying was repeated until the correct amount of washcoat was deposited on the walls of the monolith channels. The final mass of washcoat was around 20% of the total mass of the monolithic catalyst.

The samples prepared were characterized using adsorption of probe molecules to determine their available surface area and the amount of available Pt atoms.

4.1.1.1. BET specific surface area measurement

The surface area was measured by physisorption of N_2 at 77K and calculated according to the Brunauer-Emmett-Teller Theory (BET). This measurement gives a value representing the physical surface area of the catalyst without differentiating between surfaces of different chemical properties, like metal particle and metal oxide support. An automatic instrument Micromeritics ASAP2010 was used for this measurement. The measure was carried out on the coated monoliths after drying in vacuum for 2h at 225°C.

4.1.1.2. Platinum dispersion measurement

CO is a stable molecule owing to a non-bonding doublet of electrons. This property is the source of interactions between CO and transition metals. Indeed, CO forms readily strong bonds with metals and is therefore commonly used as a probe molecule to adsorb selectively on metal exposed atoms.

The CO chemisorption experiment was performed in the flow reactor described below using two CO pulses. A first 20 min pulse of gas containing 100 ppm of CO was sent over the catalyst where CO adsorbed. The sample was then flushed with Ar for 7min to remove weakly bound CO and a second pulse similar to the first flowed for 10 min. During the whole experiment, the total flow was 1L/min and the carrier gas was Ar. The uptake amount of CO was measured for the two steps. The chemisorbed CO was then calculated by subtracting the amount found on the second step from the one found for the first pulse. The number of surface Pt atoms was inferred assuming that CO adsorbed on the surface with the ratio CO:Pt= 0,8 according to the results of Foger et al [63] and Olsson et al. [64](Figure 7). The expression for the dispersion was then:

$$D_{Pt} = \frac{Pt_{exposed}}{Pt_{total}} = \frac{CO_{chemisorbed}}{N_A * m_{cat} * loading * 0{,}8}$$

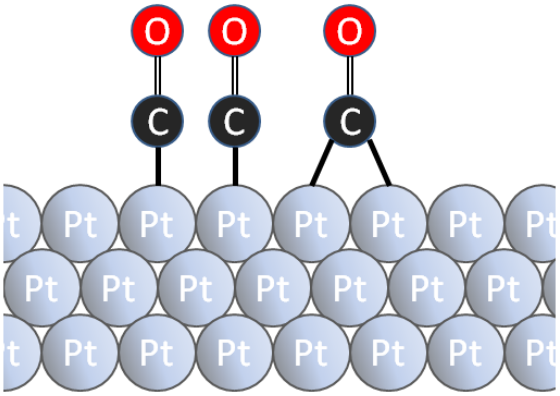

Figure 7: Schema of CO adsorption on Pt particle surface for measuring the dispersion.

There is a link between dispersion and average particle size and different relations have been proposed assuming different particle shapes. Assuming spherical particles (or hemispherical with the flat surface in contact with the support) Guo et al proposed the relation $d_{Pt} = \frac{1{,}07}{D_{Pt}}$

where d_{Pt} is the average particle size and D_{Pt} is the platinum dispersion [65]. The CO:Pt ratio was kept constant for all the analyzed data, assuming that the stoichiometry of CO chemisorption does not depend on particle size. This simplification is not fundamentally correct since the stoichiometry of CO adsorption on Pt varies between 0,6 and 1[66].

4.1.2. Reactor setup

A flow reactor was used to age (Figure 8), measure the dispersion and control the activity of the catalytic monoliths. The gas flow was supplied by a set of mass flow controllers of various floz ranges. The gases were mixed in the reactor upstream from the catalyst. The transparent tube containing the monolith and the thermocouples was made of quartz and had an inner diameter of 24mm.

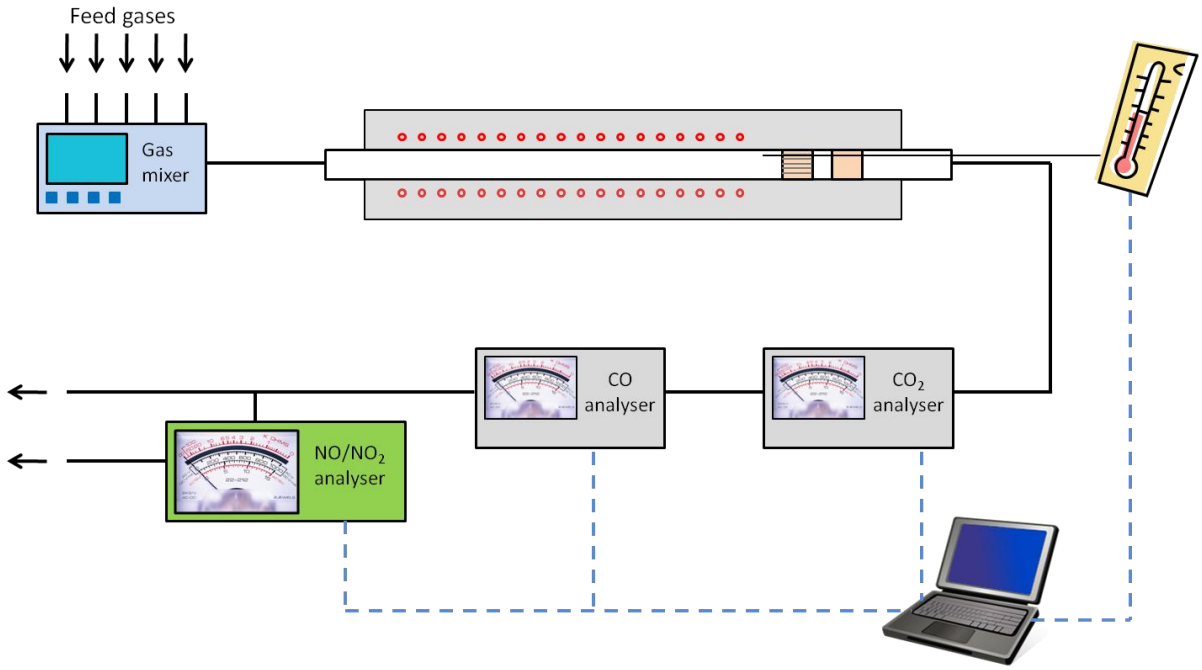

Figure 8: Schematic representation of the reactor setup.

4.1.2.1. Sample settings

To optimize the homogeneity of the gas mixture and the temperature, the catalyst was placed in the rear quarter of the quartz tube. To limit the temperature drop downstream the catalyst, which creates a temperature gradient in the monolith, a bare monolith of cordierite was placed behind the actual sample. Some experiments were run to evaluate the ability of cordierite to store molecules used in the experiments like CO and NO. Unwanted adsorption and release of compounds constitute a problem that needs to be quantified and corrected for further analysis. But cordierite did not show significant storage at room temperature. Both monoliths had the same dimensions.

4.1.2.2. Temperature control

Three thermocouples were inserted tightly through a Teflon® joint from the back of the reactor (Figure 9). Thermocouple 1 was placed in front of the catalyst and controlled the heating system to make the temperature equal to the target temperature at that position. Care was taken to place the tip of thermocouple 1 at a reasonable distance from the wall by bending the wire because the wall is in direct contact with the heating coiled resistance and is therefore thought to be hotter than the gas flow. Thermocouple 2 was placed in the center channel at half of the sample and the measured temperature was taken as the reaction/catalyst temperature. The values of the temperature represented on the x-axis of the plots refer to the temperature measured by this thermocouple. The role of the last thermocouple lying downstream was to check the temperature gradient.

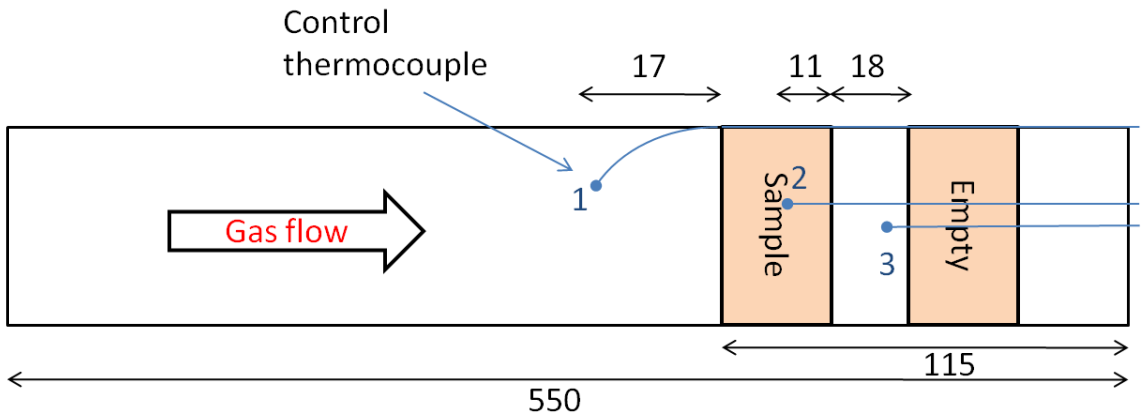

Figure 9 Schema of the flow reactor used for ageing and characterization of the DOC.

4.1.3. Flow reactor experiments

4.1.3.1. NO oxidation

The activity of every sample towards the oxidation of NO into NO_2 was controlled after each ageing step. A flow of 3000ml/min containing 500ppm NO and 8% O_2 was sent over the catalyst for 30 min at room temperature in order to reach the adsorption-desorption equilibrium of NO. Then the temperature was ramped up to 500°C at the rate of 5°C/min. The NO and NO_2 concentrations of the outlet gas was quantified by a chemiluminescence NO_x analyzer and recorded at the frequency of 1Hz.

After the ramping, the temperature was held constant for % min at 500°C to make sure that the reaction occurred at steady state. The same gas flow was maintained during the cooling. Unlike the heating, the cooling of the reactor was not carried out at a controlled rate and was faster.

4.1.3.2. Ageing under reactive atmosphere

The ageing procedure was the same for every catalyst and every ageing temperature and was performed in the flow reactor used for the activity test. Initially an Ar flow of 1000 mL/min was sent over the catalyst for 10min at room temperature before starting to heat the reactor up to the ageing temperature. As soon as the reactor temperature stabilized at the target temperature the catalyst was exposed to its respective reactive atmosphere for 2h. After this period, the ageing atmosphere was replaced by a flow of pure Ar and the reactor was cooled off. The total flow remained constant during the entire process (1000 ml/min) and only the gas composition varied from pure Ar to ageing atmosphere.

Like the heating, the cooling was as short as possible. To accelerate the cooling step, the insulation wool around the reactor was quickly removed after the 2h ageing step and compressed air was blown on the reactor tube to optimize the heat exchange with the ambient air.

In the ageing-characterization protocol, ageing was performed after the activity test, which means that the catalyst was saturated with NO_x at the beginning of the ageing step. The NO_x species were released during the heating.

4.2. Spatiotemporal study of NH_3-SCR

4.2.1. Advanced analytic technique: SpaciMS

In automotive catalysis, monolithic converters are used in order to achieve a high gas-catalyst interface and a low pressure drop. Ideally, a monolith behaves like a plug-flow reactor and concentrations of reactants and products evolve along the catalyst. These intra-catalyst evolutions cannot be detected with the usual flow reactor experiments and analytical techniques. It is of importance to know what occurs inside the catalyst in order to assess the reaction mechanisms. For example, reaction intermediates can be formed at the front of the coarse and subsequently react. Intra-catalyst measurement is a large advantage in order to investigate these features.

For this purpose the Spatially Resolved Capillary Inlet technique has been developed and was first adapted to mass spectrometer by the Oak Ridge National Laboratory and Cummins Inc. [67-71] and was later also used together with FTIR spectrometer [7]. A flexible capillary is connected to the instrument inlet and the other end is inserted into a selected channel of the monolith (Figure 10). The capillary is made of fused-silica and coated with polyimide; its outer diameter is ~150 µm. The capillary tip can be translated within the catalyst in order to determine the gas composition at any position. The extent of reaction and the possible storage onto the catalyst can then be inferred. The data collected provide useful information unmatched by other techniques. Such data are very important for comparison with kinetic models.

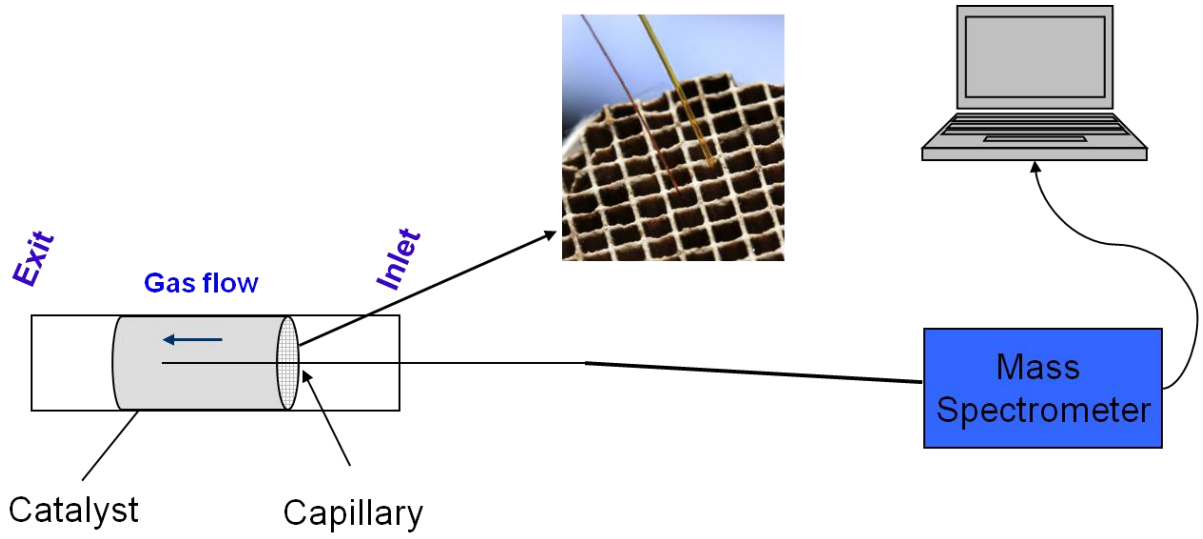

Figure 10: Schematic representation of SpaciMS system.

One difficulty with intra-catalyst measurement is the flow disturbances caused by the capillary. This effect depends on the volume of the capillary actually present in the catalyst. Thus, the outer diameter of the capillary is an important parameter. It should be much less than the channel diameter to limit the impact on the gas flow. The capillary probe pumps reaction gases, which modifies locally the concentrations of the reactants, the pressure and the flow velocity. A low sampling rate of ca. 10 µL/min limits this effect. Sà et al. [72] have investigated the intra-catalyst oscillations of the concentrations and temperature for the oxidation of CO. Using measurements and CFD simulations, they demonstrated that the intrusion of a capillary probe in

a channel had a negligible effect on the catalyst behavior. Another drawback of using a capillary inlet is the interactions between gas molecules and the inner surface of the capillary. They become non-negligible as the inner diameter of the capillary decreases and when the flow is decreasing. Interactions are greater for sticky molecules, such as NH_3 and NO_2. This can cause that the instrument response to a pulse is a more or less broad peak which complicates the time resolved analysis. Owing to this chromatographic effect, the capillary is heated and maintained at 200°C to weaken molecular interactions with the capillary walls and reduce adsorption within the capillary. Thus the time resolution is improved.

SpaciMS has been successfully used in ORNL for investigating lean NO_x-trap catalyst behavior during storage and regeneration [67, 69, 70]. The technique has been adapted to the study of fuel cells despite the difficulty caused by the formation water which can condense and eventually clog the capillary probe [71]. Other groups have performed intra-catalyst measurements on various reactions to get an insight into the spatial consumption of reactants [7, 73-75].

For the second study of this thesis, the SpaciMS technique has been, for the first time, adapted to study the reduction of NO by NH_3 according to the NH_3-SCR reaction. These experiments were conducted at Oak Ridge National Laboratory in USA.

4.2.2. Reactor setup

The micro reactor used for the NH_3-SCR study is represented in Figure 11. It was composed of two cylindrical furnaces. The larger one was the pre-heater and contained coiled pipes into which feed gases circulated to be heated up before subsequent mixing. The furnace with smaller diameter contained the quartz-tube reactor into which the catalyst was placed. Quartz rods were placed in the tube upstream and downstream from the catalyst to create gas mixing and to lower the axial and radial temperature gradients inside the reactor.

The capillary probes were inserted into the tube from the inlet (right side of the reactor on Figure 11) and K-type thermocouples were inserted from the outlet. The gas flows were metered by mass flow controllers and sent to two three-way switching valves, which were computer controlled. These electrovalves enable a fast turnaround time when switching gas stream to the reactor. The gas lines between the pre-heater and the reactor, at the outlet of the reactor as well as the capillaries were heated and maintained at a temperature above 200°C to avoid adsorption in the pipes and the formation of ammonium nitrate. Two capillary probes, the tips of which were distant of 1,25 inch, were actually used during all experiments. One capillary was placed into the catalyst, while the second was always located in front of the catalyst. Both capillaries were connected to a multiport valve, connected to the MS inlet. The gas flow from either of the capillaries could be selected for analysis and switching from one capillary to the other was made during experiment with a remote control. The inlet gas composition was consistently determined at the end of each step to get a better contrast between inlet and intra-catalyst concentrations.

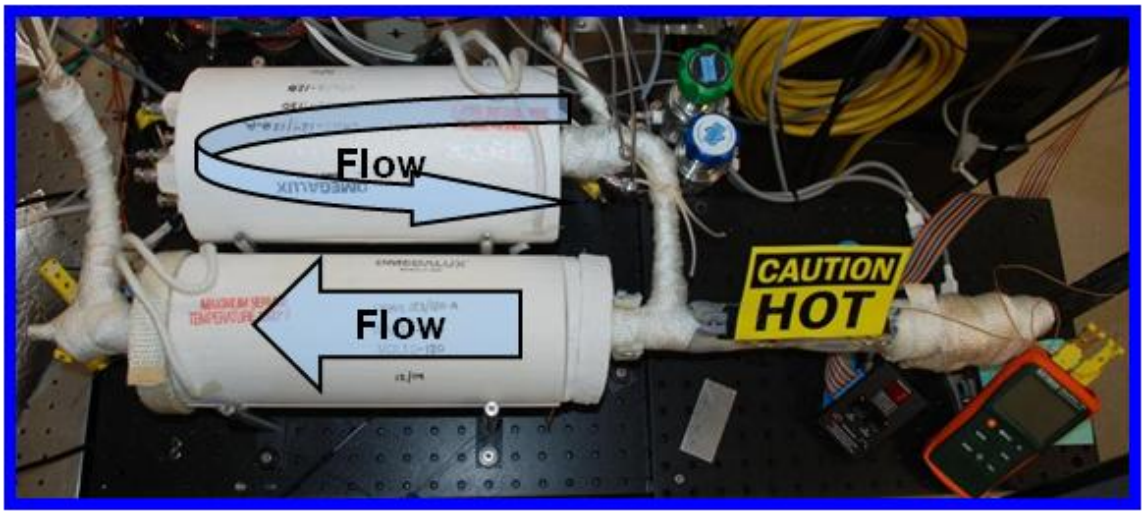

Figure 11: Picture of the reactor setup for the spatio-temporal study of NH_3-SCR at Oak Ridge National Laboratory.

4.2.3. Experimental protocol

NH_3-SCR was carried out on an Fe exchanged zeolite provided by Umicore and an Cu-Beta zeolite prepared at Chalmers containing 3,4% wt. copper. The two catalysts were characterized following a 4-step protocol developed by Cummins to study several reactions occurring in operating conditions [76]:

1- NO oxidation $2NO + O_2 \leftrightarrow 2NO_2$

2- NO reduction by NH_3 $4NO + 4NH_3 + O_2 \leftrightarrow 4N_2 + 6H_2O$

3- NH_3 oxidation $4NH_3 + 3O_2 \leftrightarrow 2N_2 + 6H_2O$

NH_3 storage in presence and absence of NO was also studied and the storage capacities of the catalysts were determined. The SpaciMS analysis gave the spatial distribution for all of these features. The 4-step protocol consisted in changing the gas composition of the feed by turning NH_3 and/or NO supply on and off in order to investigate NH_3 storage or any of the reactions mentioned above. The description of the protocol is given in Table 1.

Table 1: Feed composition during each step of the 4-step protocol (total flow 510sccm).

	NO	NH_3	O_2	H_2O	Kr
Step1 (clean)	205ppm	0	10%	5%	100ppm
Step2 (SCR)	205ppm	183ppm	10%	5%	100ppm
Step3 (NH_3 saturate)	0	183ppm	10%	5%	100ppm
Step4 (clean)	205ppm	0	10%	5%	100ppm

In order to simulate real conditions, the gas feed contained 10 % O_2, 5 % H_2O and 100 ppm Kr throughout the whole protocol. The water vapor came from liquid water heated at a fixed temperature in a hot bath. The vapor was then carried by a flow of Ar. Krypton served as reference for the mass spectrometer analysis. In the first step, 205 ppm NO was added to the base stream to clean the surface of adsorbed NH_3 as well as studying the NO oxidation. In step 2,

NO was kept in the flow and 183 ppm NH_3 was added in order to perform the SCR reaction described in section 3.1 as well as studying the dynamic of NH_3 storage in operating conditions. When the SCR reaction reached steady state, NO was turned off in step 3. In this step, the storage of NH_3 in the absence of NO was studied and the reaction of NH_3 oxidation was observed. Finally in step 4, NH_3 was switched off and NO was simultaneously started in order to observe the reaction occurring between NO flowing and NH_3 stored on the surface. The total storage capacity of the catalyst could be determined by the consumption of NO and the release of NH_3 in this last step. After the fourth step, NO and NH_3 were turned off in order to get a baseline of concentrations for subsequent calculations. The capillary was then translated to the next measurement position and the 4-step protocol could be run at this new location. Before moving on to the next position, the protocol was repeated twice and the results from the second cycle were analyzed.

5. Results and Discussion

5.1. Thermal and chemical ageing of a DOC catalyst for NO oxidation.

A series of five monoliths wash-coated with Pt/Al_2O_3 of the same batch powder, prepared as described in section 4.1.1 of the Experimental Part, was used in the comparative ageing study. They all underwent the same characterization and thermal ageing procedure reported in Figure 12. However, each monolith was treated in a different chemical atmosphere during the ageing in order to compare the effect of chemical ageing on platinum dispersion and NO oxidation performance. The reactive atmospheres tested were Ar, 10 % O_2 in Ar, 1 % H_2 in Ar, 30 ppm SO_2 in Ar and a mixture of 10 % O_2 and 30 ppm SO_2 in Ar. The samples were encoded and later referred to as "M-gas", i.e. M-Ar, M-O2, M-H2, M-SO2 and M-SO2/O2.

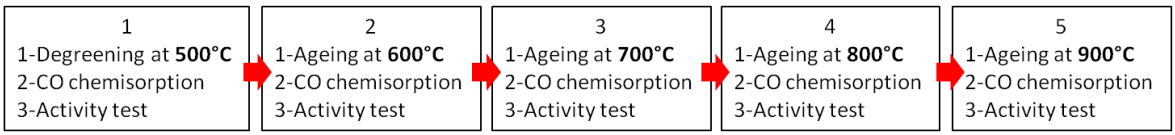

Figure 12: Scheme of step-by-step ageing and characterization.

5.1.1. Results of ageing on platinum dispersion

A typical profile obtained from our CO chemisorption experiments is presented in Figure 13. The two CO pulses led to different amounts of adsorbed CO. During the first pulse, CO is both adsorbed strongly on Pt and some weakly adsorbed CO is also stored. During the inert part after the first pulse, the weakly bonded CO is desorbed and again adsorbed during the second CO pulse.

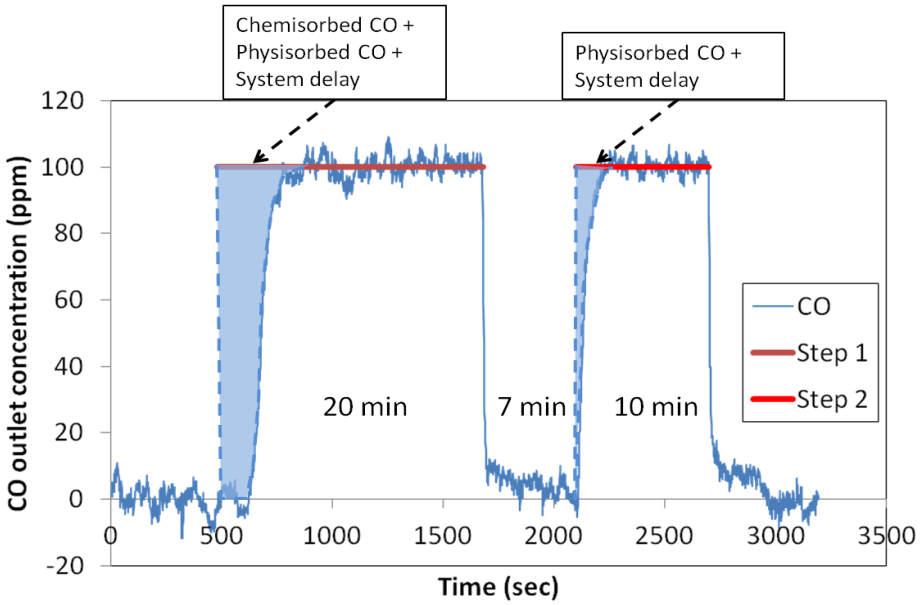

Figure 13 : CO concentration profile during dispersion measurement (M-SO_2-degreened).

High-temperature treatments result in particle growth and dispersion loss since the ratio $Pt_{surface}/Pt_{total}$ becomes smaller as the particle diameter increases. As the ageing temperature

increases, the dispersion falls. Figure 14 shows the results of dispersion after each ageing step for the reference catalyst aged in Ar. It appears that the dispersion decreased linearly until a minimum limit value of 18 % was reached after ageing at 800°C. The next ageing at 900°C did not affect the dispersion, which was stable after ageing at 800°C.

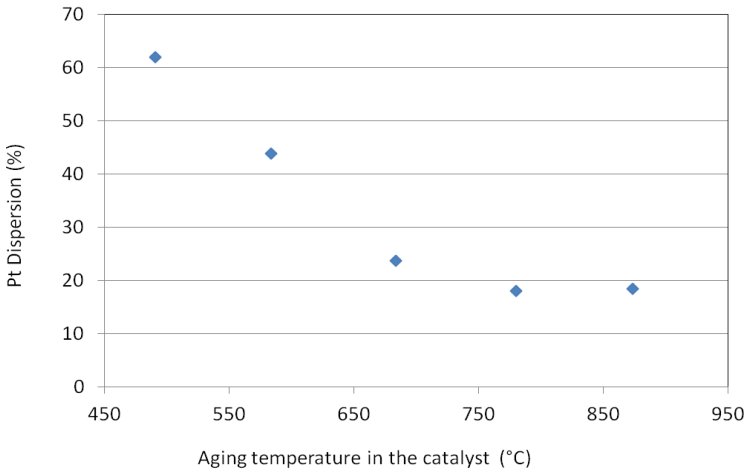

Figure 14: Evolution of Pt dispersion with ageing temperature for a catalyst aged in Ar.

5.1.1.1. Effect of H_2 and O_2

The effect of various atmospheres on the sintering was investigated using the same conditions as the case of ageing in Ar, in order to facilitate a comparison. Results of ageing in oxidative (10% O_2) and reductive atmosphere (1% H_2) are shown in Figure 15. Since the formation of migrating platinum species is not favored in H_2, the effect of H_2 was to limit the sintering at low ageing temperatures (600°C). However, the sintering was activated at higher temperature and the final dispersion (15%) was comparable to the dispersion of the reference sample (18%).

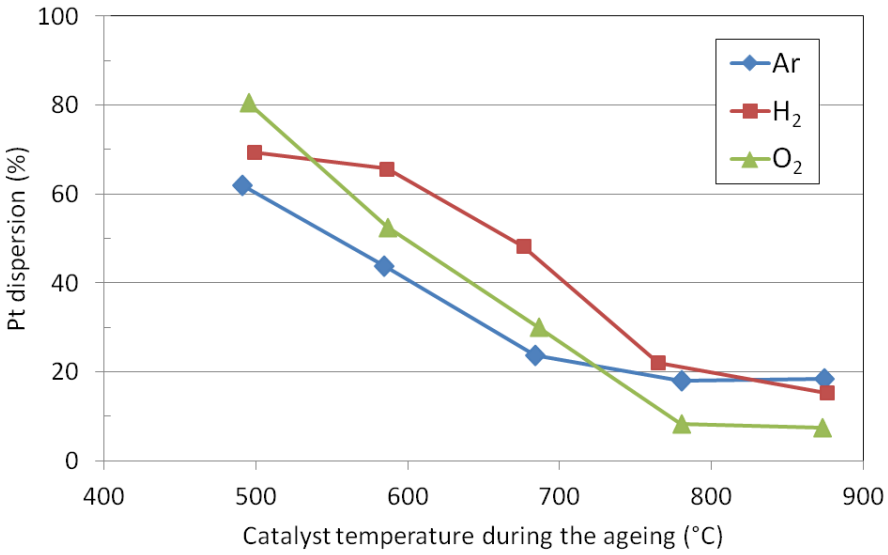

Figure 15: Evolution of dispersion for ageing in 10% O_2 and 1% H_2 and comparison with the reference case (Ar)

In O_2, the dispersion loss is linear as in Ar and the slopes of the two curves are very similar until ageing at 700°C. The main effect exhibited is the ability of oxygen to lower the minimal limit of dispersion. At high temperature, oxygen can form volatile Pt oxide, which is more mobile and sintering can continue further than in Ar, when large particles are distant from each other. Only a one-percent dispersion loss (from 8% to 7%) was noted during the last ageing stage at 900°C in O_2, suggesting that the limit is practically attained after ageing at 800°C.

5.1.1.2. Effect of SO_2

Important sintering of platinum has been observed at low temperature during the NO oxidation experiment when the feed contained a small amount of SO_2 [59]. In order to correlate the presence of SO_2 to low-temperature sintering and confirm this finding, two samples were aged in 30 ppm SO_2 and a mixture of 30 ppm SO_2 + 10 % O_2, respectively. The dispersion of these two catalysts is compared with the dispersion of the reference catalyst in Figure 16.

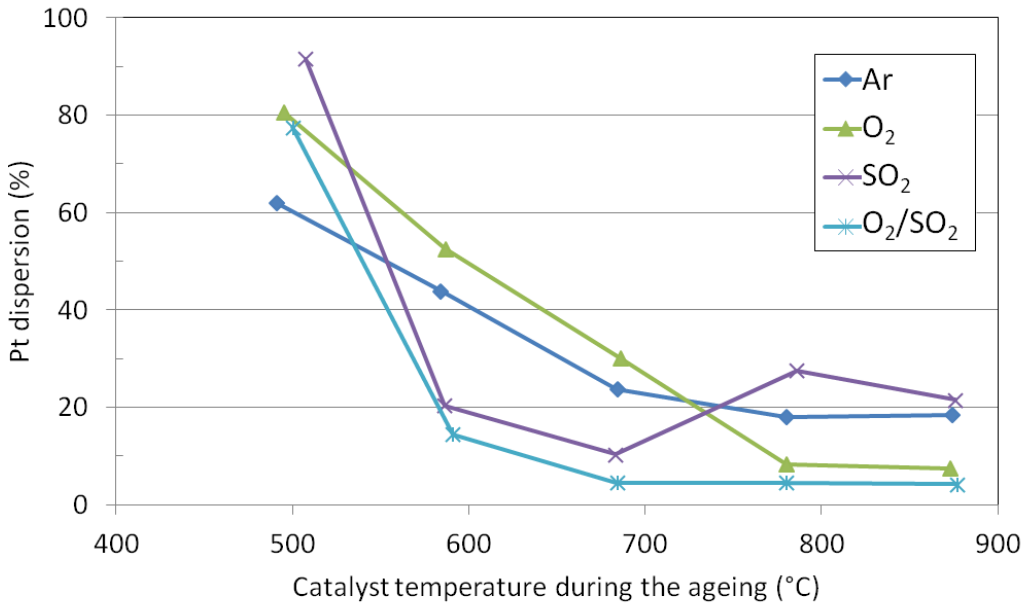

Figure 16: Evolution of the dispersion of catalysts aged in 30 ppm SO_2, 30 ppm SO_2 + 10 % O_2, Ar and 10 % O_2.

Since the dispersion of both SO_2-aged samples dropped after the first ageing stage at 600°C, SO_2 had a very important effect on sintering. The initial dispersion fall led to a value less than 20 % that was comparable to the final dispersion of the Ar-aged catalyst. This result confirmed the promotion of sintering by SO_2 at low temperature. However, we observed an increase in the dispersion for M-SO2 after ageing at 800°C. The reason might be that there were residues of sulphur left on the platinum sites that resisted the reduction treatment prior to the CO chemisorption. Thus, the number of platinum sites available for CO chemisorption may have decreased due to sulphur coverage, leading to low apparent dispersion. It is also possible that a real redispersion effect has taken place. This feature was not observed for the SO_2/O_2 mixture. Attempts of redispersion of sintered catalysts (M-Ar and M-O2) with SO_2 at 800°C were performed and no increase of metal dispersion was observed. More investigations are needed to understand this phenomenon which was reproduced on two samples aged in SO_2.

The adsorption and desorption of SO_2 on Pt single crystals and platinum-supported catalysts have been studied [55, 77-81]. It seems that on metallic Pt, SO_2 desorbs easily at relatively low temperature. Thus, Zebisch et al. [81] showed that SO_3 decomposes at 500K and adsorbed SO_4, while more stable, desorbs at 650K on the Pt(110) surface. Streiber et al. [80] calculated a zero SO_2 coverage from 400K on the Pt(111) surface. The temperatures evoked are lower than the reduction temperature (400°C) applied to our catalysts prior to CO chemisorption , which is why we expect the complete removal of adsorbed sulfur compounds. However studies on real catalysts mentioned higher desorption temperature ranges [22, 55, 77, 78]. The formation of stable sulfates and sulfides which decompose and slowly desorb at high temperature occurs on the metal oxide support. The desorption temperature range varies with the type of support used and, in the case of aluminum sulfates, can be as high as 1000°C [55]. Apesteguia et al. [77] observed that Pt catalyzes the reduction of aluminum sulfates with H_2. They observed a reduction at 450°C assigned to sulfate reduction but no simultaneous desorption of product,

namely H_2S, which took place when 600°C was reached. They ascribed this observation to the formation of H_2S adsorbed on Pt.

The literature results are somewhat contradictory, and it is, therefore, difficult to know whether sulfur species have occupied a fraction of platinum sites during CO chemisorption after low temperature ageing. It is likely that aluminum sulfates were still present on the support surface and that some platinum atoms were free of sulphur, since they were detected by CO chemisorption.

After the whole ageing procedure was completed, M-SO2/O2 presented the lowest dispersion among all catalysts. Moreover, its final value was already reached after the second ageing step at 700°C, suggesting a fast sintering at low temperature. It can be concluded that this treatment combines the effect of oxygen, i.e. low minimum dispersion and the effect of SO_2, with a high sintering rate at low ageing temperature.

5.1.2. Results of ageing on catalytic activity

The activity of the catalyst was affected by thermal ageing as well, but unlike the dispersion, NO conversion increased after ageing. The results of the NO oxidation activity tests for M-Ar are shown in Figure 17 (left panel), where the increase of the maximum conversion, as well as the broadening of the temperature window after each aging stage, can be witnessed. The values for the maximum conversion reached were determined and shown on the right panel where a linear relation with respect to the ageing temperature is noted. NO oxidation is a structure sensitive reaction that is much faster on larger particles than on smaller ones for a Pt-supported catalyst. Thus, in general, thermal ageing, because it results in particle growth, enhances the catalyst performance.

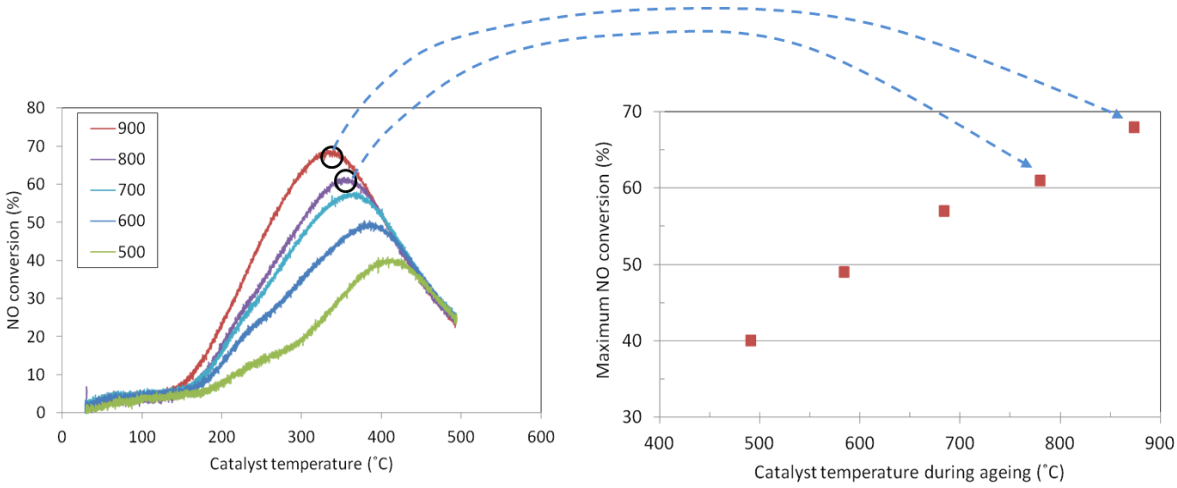

Figure 17: NO conversion after ageing step at 500 (degreening), 600, 700, 800 and 900°C (left) and evolution of the optimal conversion (right) in the case of a catalyst aged in Ar.

5.1.2.1. Effect of H_2 and O_2

Ageing in H_2 and O_2 resulted in slightly different behavior regarding the evolution of dispersion compared to the effect of inert atmosphere (see 5.1.1.1). The same comparison was made for the NO oxidation activity tests and the results are presented in Figure 18.

After the moderate increase in activity upon the first ageing step, M-H2 showed linear behavior similar to M-Ar. It is, however, worth noting that the conversion of M-H2 after full ageing was 10 % higher than for M-Ar. The activity progression of M-O2 took on a totally different shape and increased tremendously after the ageing at 600°C, passed through a maximum point and was practically depleted at higher ageing temperatures. In fact, after the first stage, M-O2 was more efficient than fully aged M-Ar. Ageing in O_2 resulted in platinum particles that were much more active for NO oxidation. However, the deactivation observed after higher aging temperatures were likely caused by the formation of Pt oxide, which could have been facilitated on particles that were grown in presence of O_2.

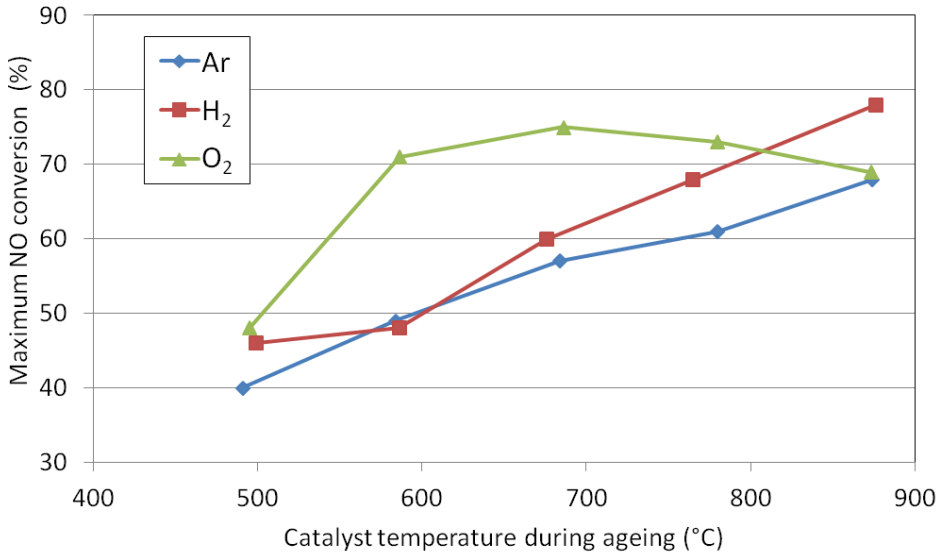

Figure 18: Comparison of activity of catalysts aged in Ar, 10 % O_2 and 1% H_2.

5.1.2.2. Effect of SO_2

The effect of SO_2 and the combination SO_2+O_2 on the activity is addressed in Figure 19 where the results of M-O2 and M-Ar are also plotted to facilitate a comparison. The two catalysts aged in SO_2 and SO_2+O_2, respectively, exhibit different trends for the NO oxidation activity. However, both samples had a high (>80%) and comparable activity at the end of the ageing procedure. The change in activity between M-Ar and M-SO2 is similar after the first ageing while the activity stayed below 50%. However, as the ageing progressed, the rise in activity was sharper for the M-SO2 sample and after 900°C the NO oxidation activity was 20% higher for M-SO2 than for M-Ar.

M-SO2/O2 behavior was greatly influenced by the presence of O_2 since its activity initially rose abruptly, following the curve for M-O2. After higher ageing temperatures, the performance of M-SO2/O2 kept improving (except after 900°C), while M-O2 underwent deactivation already at about 800°C. The activity of M-SO2/O2 seemed to exhibit a similar behavior of M-O2 for the lower ageing temperature, before the influence of SO_2 started to dominate and resulted in further increased M-SO2/O2 activity.

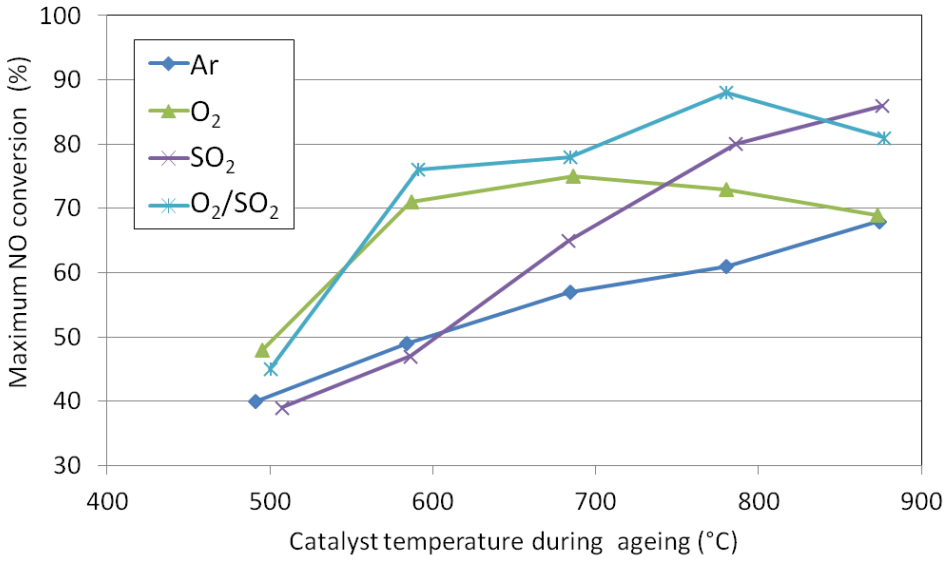

Figure 19: Evolution of maximum NO oxidation activity of catalysts aged in Ar, 30 ppm SO_2, 30 ppm SO_2 + 10 % O_2 and 10 % O_2.

Finally, it should be stressed that the best activities were found for the catalysts aged in sulfur-containing atmospheres which exhibited much better performance than catalysts aged in Ar, O_2 and H_2, especially at an advanced ageing state. This result confirms the beneficial effect of SO_2 on NO oxidation and provides a mean for improving the yield of Diesel oxidation catalysts.

5.1.3. On the effect of chemical ageing on NO oxidation performance

It is observed that NO oxidation is structure sensitive and higher a rate is obtained for larger particles. Therefore, decreasing the dispersion would increase the activity. However, it is not only the platinum dispersion that controls the NO oxidation activity; the situation is much more complex. One goal of the present study is to reveal specific differences of catalytic activity attributable to the reactive atmosphere during ageing. The ageing atmospheres tested in this study showed various impacts on catalyst activity. These impacts have to be compared with the simultaneous evolution of dispersion to be ascribed either to a particle size effect or an intrinsic chemical effect.

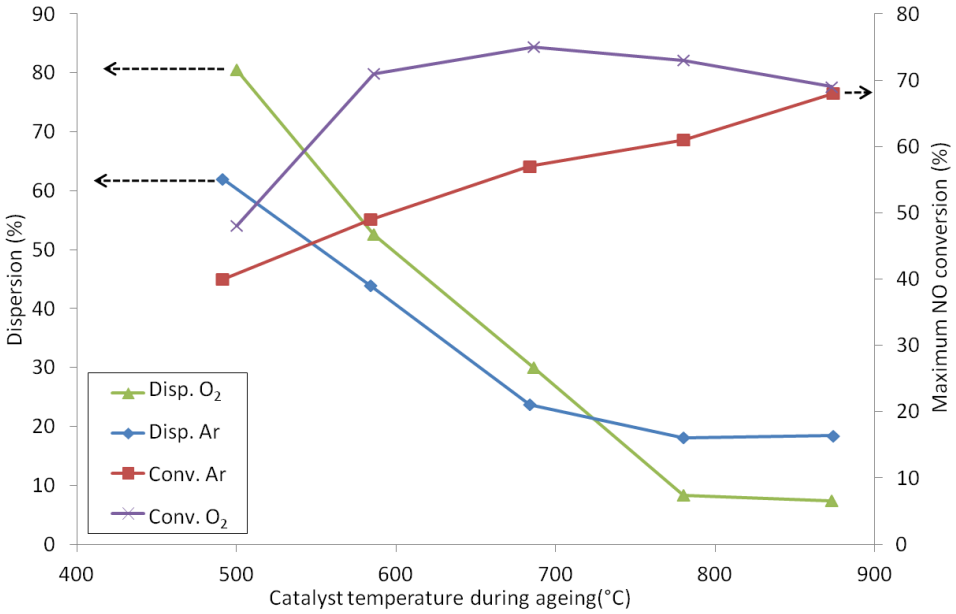

Figure 20: Comparison of dispersion and activity trends for catalysts aged in 10 % O_2 and in Ar.

Figure 20 clearly shows the specific effects of oxygen on activity. Indeed, while the dispersion of M-O2 followed the same pattern as M-Ar dispersion, its activity exhibits a totally different trend. After the initial ageing, the dispersion loss and the dispersion of both catalysts were similar but M-O2 showed a maximum NO oxidation activity of about 70% compared to only 50% for M-Ar. In that case, it can be ruled out that only the particle size determines the activity. Moreover the dispersion of M-O2 dropped from 30 to 8% after ageing at 800°C, while the activity lowered. It can be concluded that oxygen has an effect on NO oxidation which is not attributable to an increase of particle size. Ageing in O_2 at low temperature creates greater particle activity without severe sintering while ageing at higher temperatures results in less active particles, which might be attributed to platinum oxide formation.

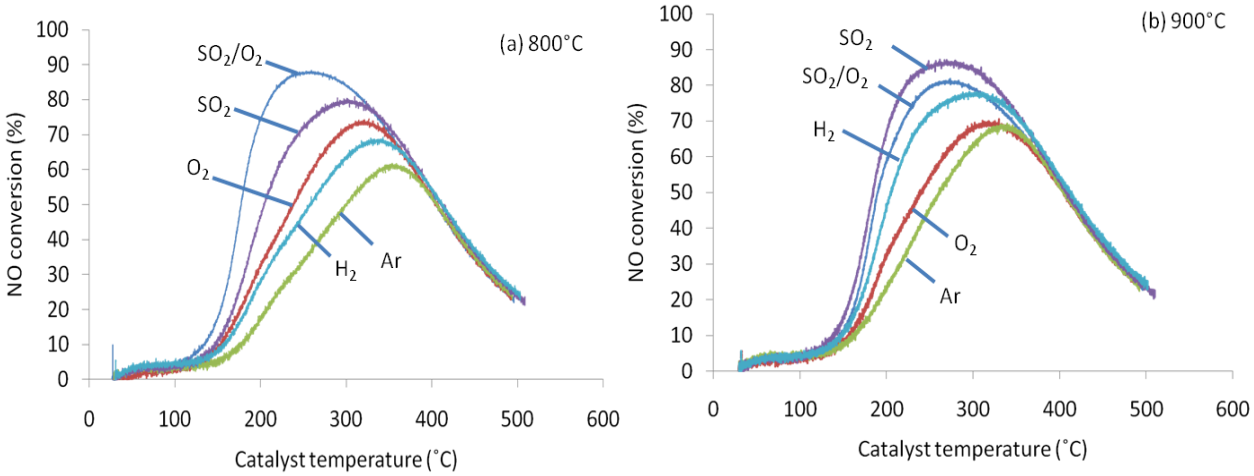

Figure 21: Activity profiles of all catalysts before (a) and after (b) the last ageing at 900°C.

In Figure 21, the NO oxidation activity profiles for all catalysts are shown after aging at 800°C (left panel) and 900°C (right panel), respectively. After 800°C, the catalysts could be classified regarding their activity in the following order: M-SO2/O2 > M-SO2 > M-O2 > M-H2 > M-Ar. At this stage, the dispersion of all catalysts was low and stable although a minor decrease was measured for M-H2 and M-SO2 after the last ageing step at 900°C. Thus, it can be considered that any change in activity occurring during the last ageing was due to the atmosphere effect. As shown in Figure 21, the classification established for 800°C-aged catalysts was not valid after ageing at 900°C where the activity of M-Ar, M-H2 and M-SO2 kept increasing while the performance of M-O2 and M-SO2/O2 decreased. The new order was as follow M-SO2 > M-SO2/O2 > M-H2 > M-O2 > M-Ar.

5.2. Spatio-temporal study in operating conditions of a Cu-Beta zeolite for NH_3-SCR

As described in section 4.2.3, the properties of the catalyst were studied through a protocol that consists of four steps (Step 1: $NO+O_2+H_2O$, Step 2: $NO+NH_3+O_2+H_2O$, Step 3: $NH_3+O_2+H_2O$ and Step 4: $NO+O_2+H_2O$). The concentration profiles obtained for an entire experiment at 325°C and at 0.5L from the SpaciMS are shown in Figure 22. The capillary position was determined using NH_3 oxidation and SCR profiles, which is described in detail in Paper II.

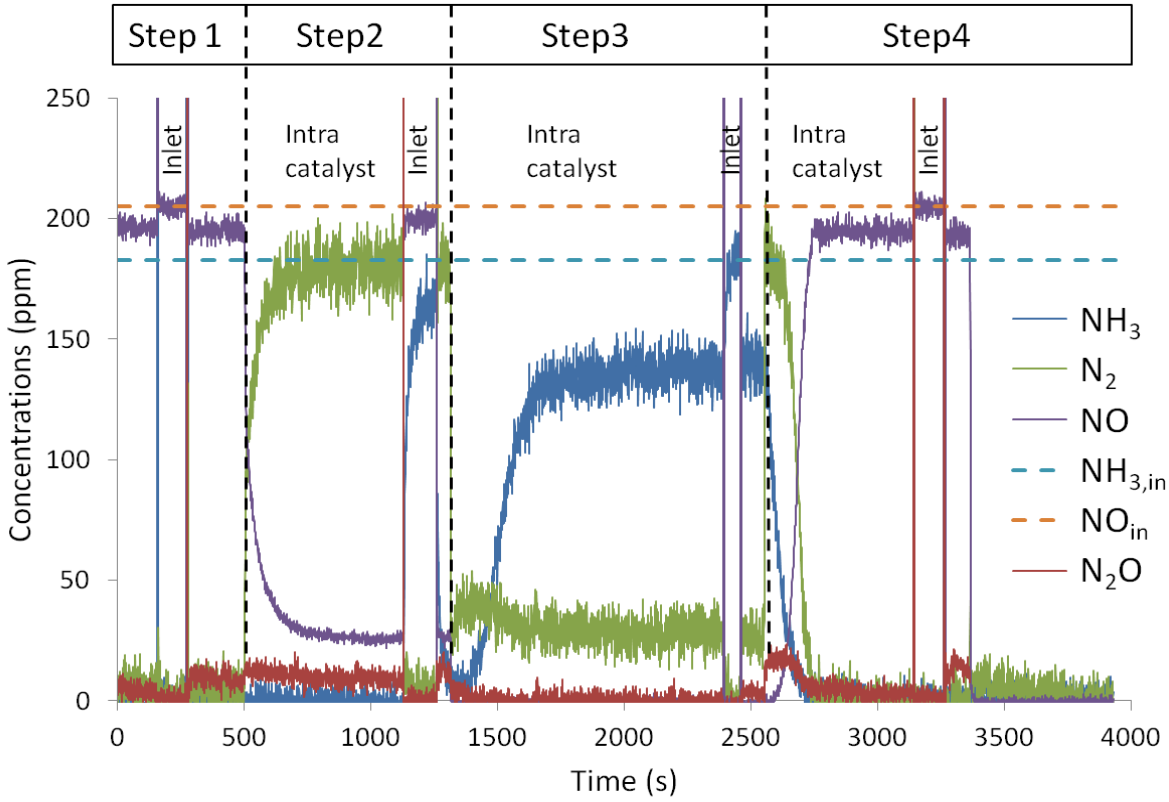

Figure 22: Concentration profiles obtained for experiment at 325°C at 1/2L location.

5.2.1. Oxidation performance

5.2.1.1. NO oxidation

The catalyst NO oxidation ability was assessed from step 1 of the protocol, when a fraction of NO was consumed and oxidized into NO_2. As seen, intra-catalyst NO concentration was lower than inlet NO concentration, indicating NO consumption inside the sample. NO_2 concentration went up at the beginning of step 1 and reached a steady state value. A steady state conversion could be deduced from NO consumed and is shown in Figure 23 for all locations. The oxidation of NO increased quite linearly within the first half of the catalyst at both 325°C and 400°C, while a much smaller increase was noted for the rest of the catalyst. A maximum NO conversion of 22% was found at 400°C at the outlet, which is still far from the equilibrium. Despite the favorable thermodynamics for NO_2 at lower temperature, the maximum conversion is only around 5% at the outlet at 325°C. The reason is that the NO oxidation was, in these cases, kinetically limited. At 200°C, no oxidation was observed. It can be concluded that the Cu-Beta

catalyst studied was able to catalyze NO oxidation with a poor efficiency characterized by a high ignition temperature and a low conversion relative to the thermodynamic equilibrium. This reaction became non-negligible at high enough temperatures, like 400°C. The low conversion observed in the rear half of the catalyst was likely due to a lower rate when equilibrium was approached.

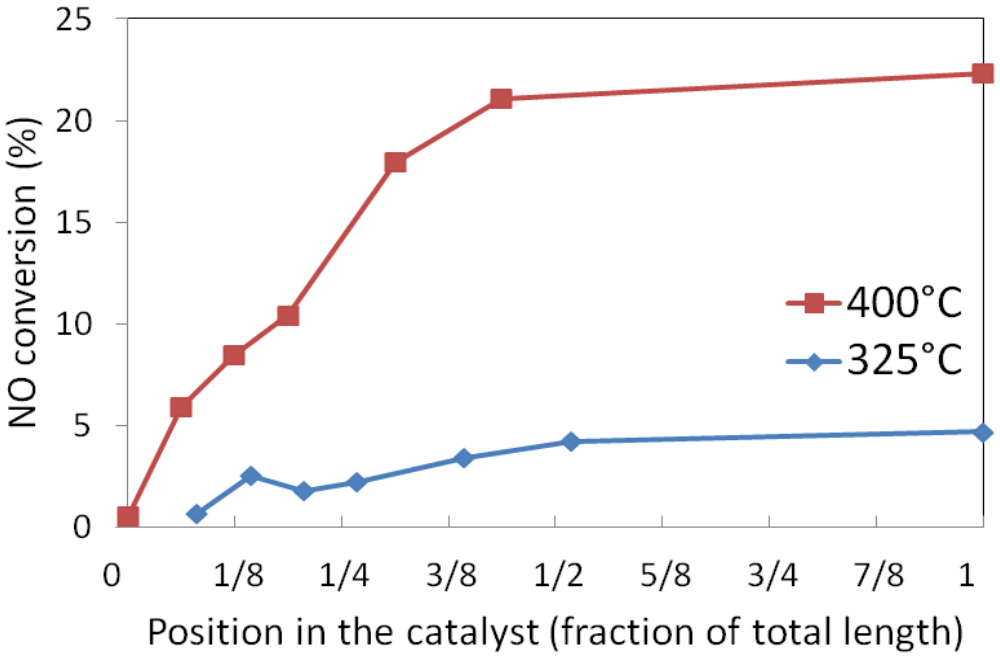

Figure 23: Intra-catalyst NO oxidation at 325°C and 400°C.

5.2.1.2. NH_3 oxidation

Copper-based catalysts are known to oxidize NH_3 at quite a low temperature [82]. In step 3, NH_3 oxidation with oxygen according to reaction (7) was examined. The conversion, defined as the ratio between consumed NH_3 and NH_3 in the feed, was calculated at steady state at each location. The results for 325 and 400°C are shown in Figure 24. At 325°C, the conversion increased linearly throughout the catalyst to eventually reach 45% in the outlet. At 400°C, the reaction was much faster and 100% NH_3 conversion was attained by 7/16 length of the catalyst.

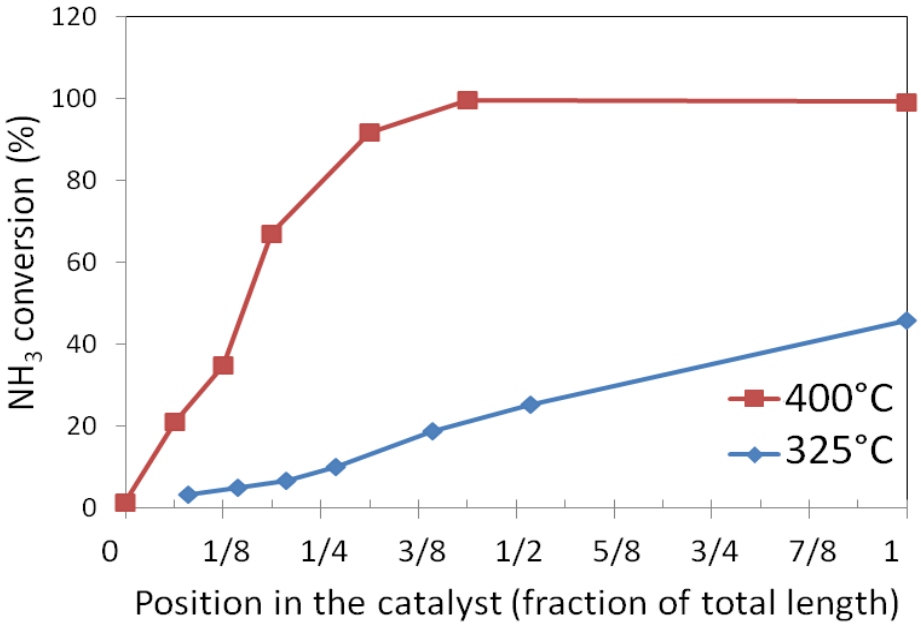

Figure 24: Intra-catalyst NH_3 oxidation at 325°C and 400°C.

At 200°C, no significant NH_3 conversion was observed. NH_3 oxidation was greatly enhanced by the temperature, with no reaction at 200°C and total conversion at 400°C. The oxidation of NH_3 by oxygen should be limited in SCR conditions, because NH_3 used for reducing NO_x is depleted. This side reaction during SCR has been observed also on other catalysts and was responsible for their lower activity at high temperature. N_2 was the only product observed in step 3 indicating that NH_3 was oxidized according to reaction (7) and did not form NO nor N_2O.

5.2.2. Spatial evolution of SCR reaction with ammonia

The spatial distribution of the SCR reaction was determined from step 2; the effect of temperature, the selectivity and the stoichiometry of the reaction were addressed. The inlet feed gas consisted of 183 ppm NH_3, 205 ppm NO, 10% O_2 and 5% H_2O. Thus, the conversion was limited by the amount of ammonia available and, according to the stoichiometry of standard SCR reaction (reaction (1)), the maximum NO consumption was only 183 ppm. The NH_3-limited NO conversion is defined as follows:

$$\chi = \frac{NO_{consumed}}{NO_{feed}} * \frac{205}{183}$$

The reason for showing the conversion in this manner is to clarify the stoichiometry of NO and NH_3 during the reactions.

5.2.2.1. Temperature effect

In Figure 25, the NO, NH_3, N_2 and N_2O concentrations are shown for 325°C. During the SCR step, both NO and NH_3 steady-state concentrations decreased, as illustrated by Figure 25. NH_3 was eventually fully depleted. As expected, NO concentration was never zero and remained stable

after total consumption of NH_3. The product was mainly N_2 but small amounts of N_2O were also detected.

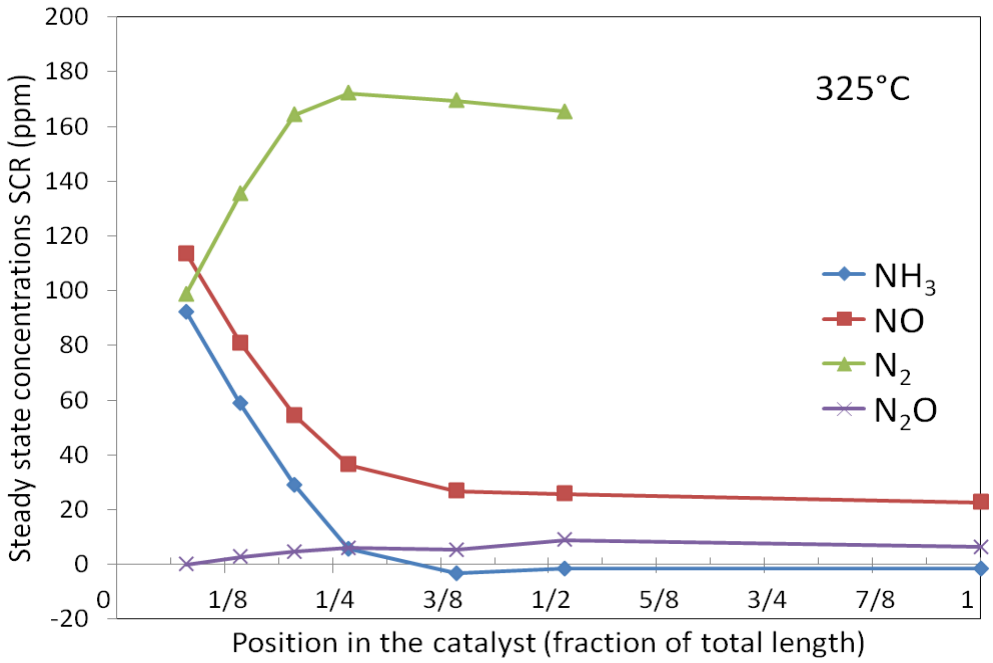

Figure 25: NO, NH_3, N_2 and N_2O steady-state concentrations during SCR at 325°C.

The uncorrected NO conversion profiles at 200, 325 and 400°C are reported in Figure 26 and illustrate the temperature dependence of reaction rates. The SCR reaction was faster at 400°C while it was slower at 200°C, but the maximum conversion was reached at the outlet at the three temperatures. It points out the advantage of SpaciMS over effluent-based analysis which would make impossible to detect this rate variation. The conversion increased linearly in the front of the catalyst within the so-called *SCR zone*, i.e. the volume in which NH_3-SCR reaction occurs until NH_3 is fully consumed. As the temperature increased, the reaction rate became higher and the limit of the SCR zone was progressively shifted to the catalyst front. Most of NO was reduced within 3/16 and 1/4 of the total catalyst length at 400 and 325°C, respectively, while the full catalyst is used to oxidize 100 % of NH_3 (and reduce equivalent amount of NO) at 200°C.

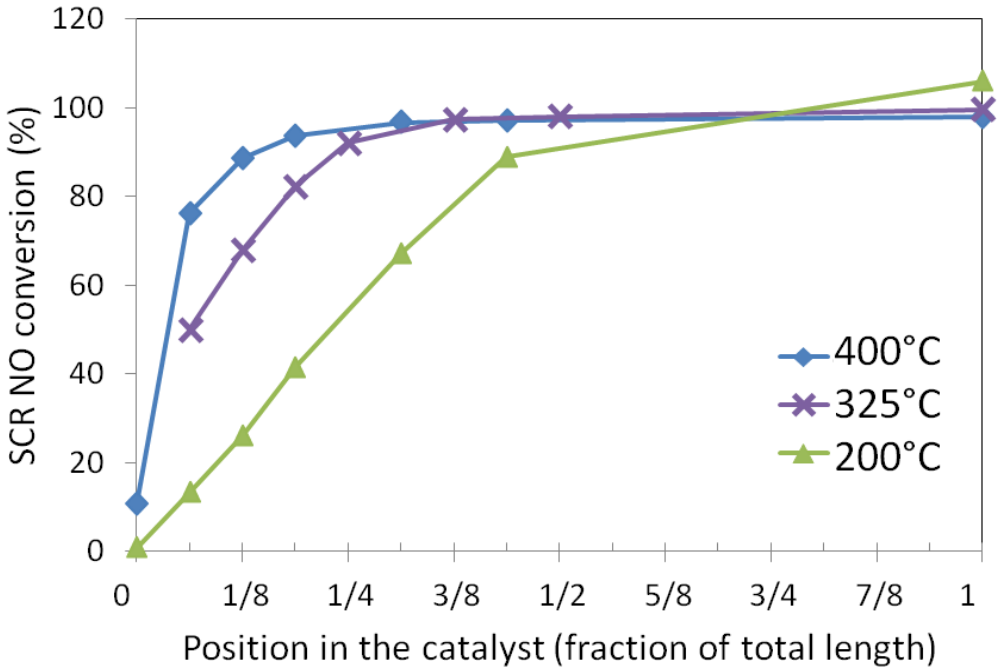

Figure 26: NO conversion profiles in SCR at 200, 325 and 400°C.

5.2.2.2. Selectivity

As shown Figure 24 and previously mentioned, Cu-exchanged zeolites are able to oxidize NH_3 in a NO_x-free environment according to reaction (7). This reaction competes with the SCR reaction in the presence of NO_x and a good selectivity towards the SCR reaction is demanded in order to optimize the process and limit NH_3 consumption. In order to assess the selectivity of the catalyst, NH_3 conversion and NH_3-limited conversion of NO at steady state are represented throughout the catalyst in Figure 27 for all three temperatures (200, 325 and 400°C). It can be seen that at 200 and 325°C, the ammonia-limited conversion of NO and the ammonia conversion followed each other. These results show that as much NO as NH_3 was consumed, thus the stoichiometry was 1:1, which is the case for the standard SCR reaction (reaction (1)). At 400°C the conversion of ammonia was slightly higher, due to ammonia oxidation. However, the SCR reaction rate was significantly larger than the side reactions rate in the investigated temperature range.

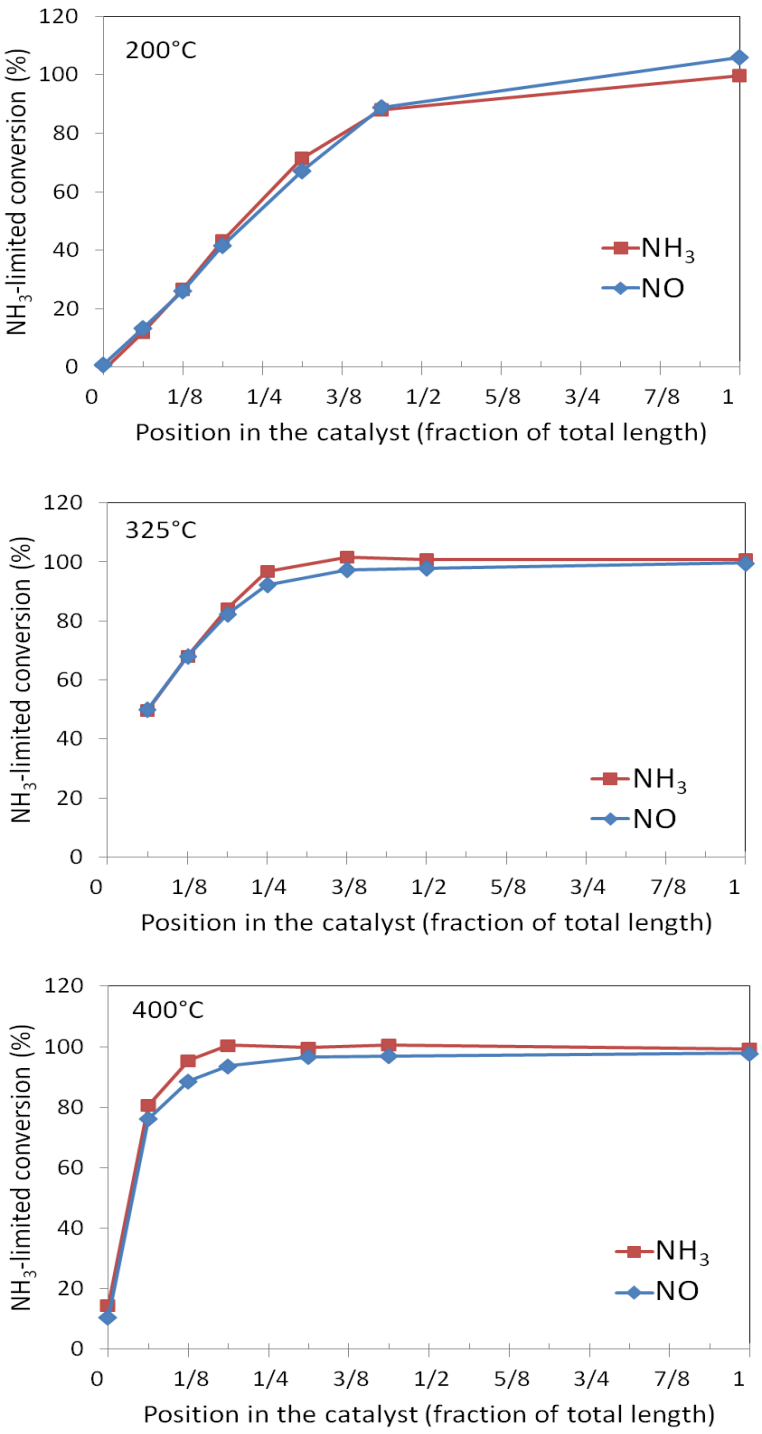

Figure 27: NH_3-limited NO conversion and NH_3 conversion during SCR at 200, 325 and 400°C.

Figure 28 represents the N_2O concentrations during SCR and shows that the amount of N_2O increased sharply in the front of the catalyst before leveling off in the back half of the catalyst, which was consistent with the SCR zone. The N_2O production was generally quite low, with the maximum observed at 200°C at the outlet. N_2O profiles were similar at 200 and 400°C, while the production was lower at 325°C. N_2O formation at low temperature has been attributed to

ammonium nitrate formation and decomposition [3, 8, 83]. At high temperature, N_2O formation may involve NO_2 formation and subsequent NH_3 oxidation by NO_2 [3, 7, 10]. More specifically on Cu-zeolite catalysts, Delahay et al. proposed that N_2O formation occurred on Cu-dimer bridge-bonded by one oxygen atom [83] according to the latter pathway; these types of active sites were also suggested by Komatsu et al. [9] for NH_3-SCR.

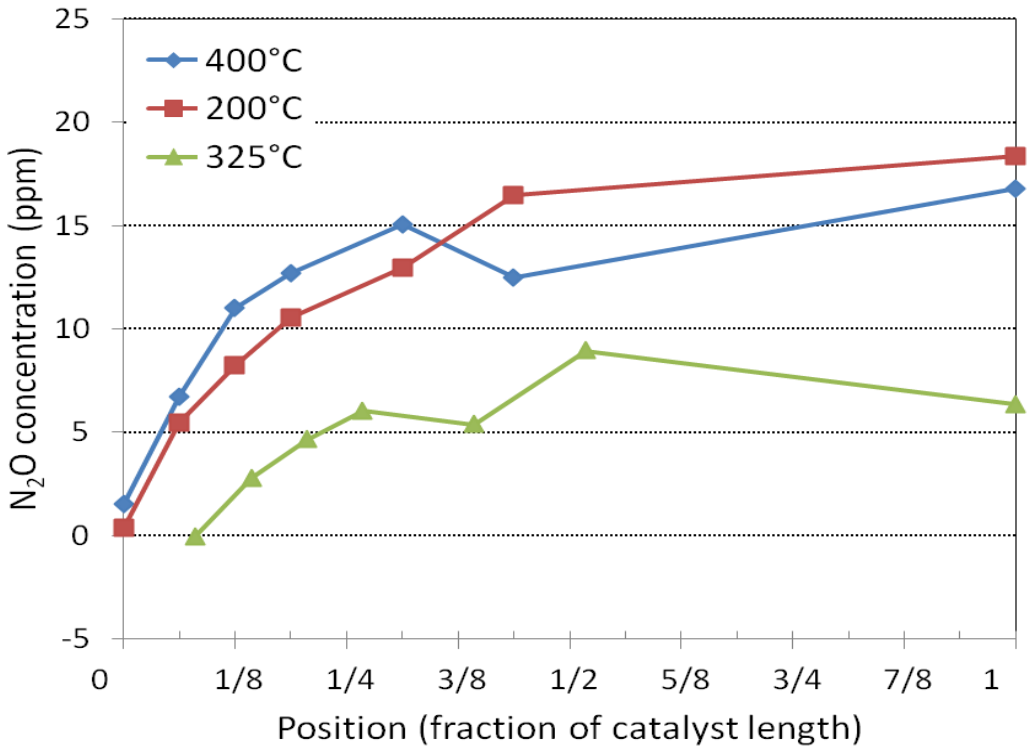

Figure 28: Steady-state N_2O concentrations during SCR at 200, 325 and 400°C.

5.2.3. Spatial distribution of ammonia storage

NH_3 is a Lewis and Brønsted base and interacts with acidic functions. Zeolites have an acidic nature and can, therefore, store NH_3. NH_3 storage capacity is an important feature to SCR catalysts since the catalyst can be used as a buffer by storing excess of NH_3 since the NH_3 slip, i.e. NH_3 exiting the catalytic system, must be minimal. Stored NH_3 can then react with NO according to SCR if NO production of a car were to increase punctually and suddenly. Thus, using zeolite for NH_3-SCR enables to store excess NH_3 and provide extra NH_3 when needed. In our experimental protocol, NH_3 storage capacity can be deduced from studying the dynamic variations. Step 2 revealed that NH_3 was able to be stored during SCR, highlighting the competition between storage and SCR for NH_3. The saturation of the catalyst during step 3 and the subsequent cleaning of the surface by NO in step 4 provide information on the total storage capacity of the catalyst.

5.2.3.1. Ammonia storage calculations

Three storage capacities were defined by Kamasamudram et al. [76] including dynamic capacity (DC), unused capacity (UC) and total capacity (TC). They are directly measurable from the 4-step protocol. DC refers to the amount of ammonia trapped during SCR operation, i.e. step 2 (see

(Figure 29). UC is the storage capacity not used during SCR and consequently available when step 3 starts. Finally, TC is measurable in step 4 and is the sum of two components: NH_3 released from the surface and NH_3 reacting with NO according to the standard SCR.

The capacities are quantitatively determined by integrating the corresponding area of the concentration profile illustrated in Figure 29. The results are limited to analysis at 200 and 325°C since storage at 400°C is very limited.

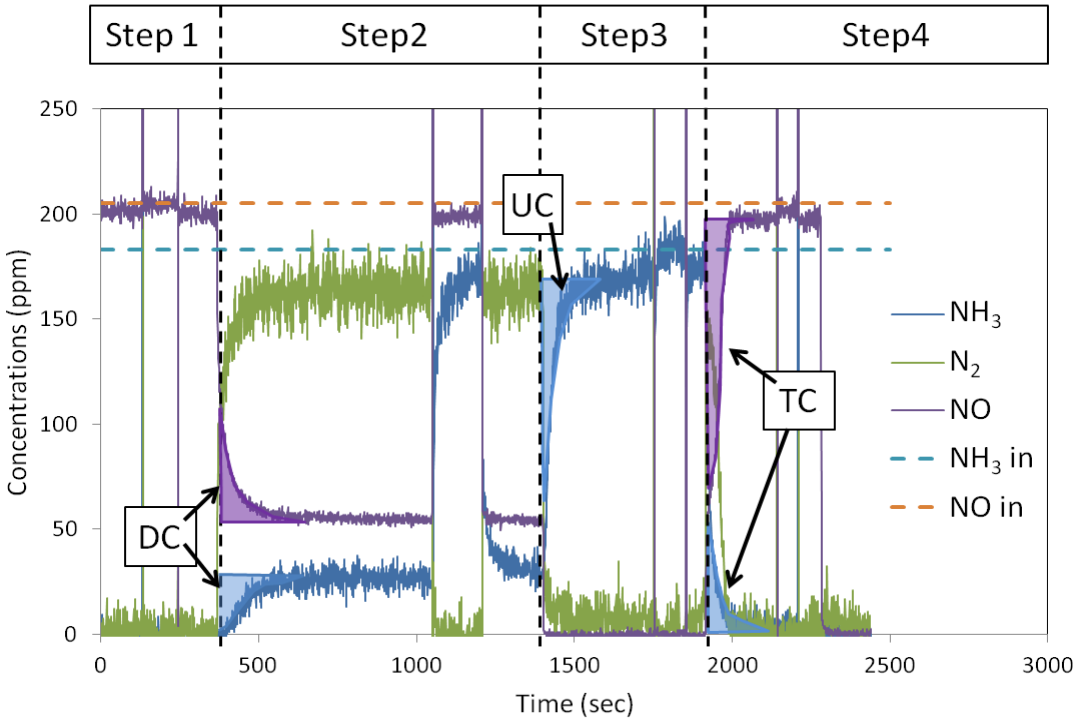

Figure 29: Illustration of integration method for capacity calculations (at 325°C and 3/16L location).

The main difficulty of calculating NH_3 storage derives from the integration of NH_3 signal over the dynamic zones. Indeed, while the time response of N_2 and NO is very fast, NH_3 presents a slower time response and shows a non-step-like response when its concentration rises and a tail when its concentration suddenly decreases. This behavior is seen in Figure 29, when switching to the inlet capillary. Empty reactor experiments were used to correct for this behavior, something that is described in detail in Paper II. The method would slightly overestimate the DC for the cases with higher ammonia conversion, as discussed in Paper II. DC, measured in step 2, is the sum of two areas obtained by the integration of NO and NH_3 concentration, respectively (Figure 29). It is assumed that at any time during step 2, the following reactants mass balance would be valid:

$$NO_{feed} + NH_{3,feed} = NO_{out} + NH_{3,out} + NH_{3,stored} + 2 \times NH_{3,reacted}$$

With NO_{feed} = 205 ppm, $NH_{3,feed}$ = 183 ppm and where $NH_{3,stored}$ is the instant NH_3 storage which is equal to zero at steady state. If the SCR reaction rate were the same during the entire step 2, the area marked in blue in Figure 29 would be the amount of stored ammonia. However, when the coverage of the ammonia on the surface is lower in the beginning of step 2, the SCR rate is also

lower and the amount of ammonia storage is, therefore, underestimated. The NO profile is a measure of the SCR reaction, assuming small amounts of NO adsorbed on the surface. Thus, when adding the two areas marked in Figure 29, the dynamic capacity is obtained. NH_3 slow response has a contribution to DC which becomes negligible at high DC even though it is not constant.

The total capacity (TC) is measured in step 4 according to the same integration method as for DC (Figure 29). A part of the NH_3 tail is due to the slow response and becomes significant at low TC but, the NO signal contribution is considered exact.

5.2.3.2. Distribution of ammonia storage capacities

Figure 30 displays the spatial distribution of DC and TC at 200 and 325°C. The general trend is that TC increases linearly along the catalyst, which is expected for a catalyst with homogenous distribution of the active sites. Secondly, DC and TC are similar in the front of the catalyst indicating that all storage sites in this zone are completely filled by NH_3 during SCR operation, which highlights the competition between storage and SCR under transient operation. The TC and DC curve separate at 1/2 and 1/4 location at 200 and 325°C, respectively. Interestingly, these locations correspond to the point where 100 % conversion is reached. Within this zone, SCR occurs until NH_3 is fully consumed. For that reason, no NH_3 flows beyond this zone in the gas phase and it seems consistent that DC cannot increase further. This zone is defined as "the SCR zone" and our capacity and SCR results show that as the operating temperature increases, it shifts progressively to the catalyst front.

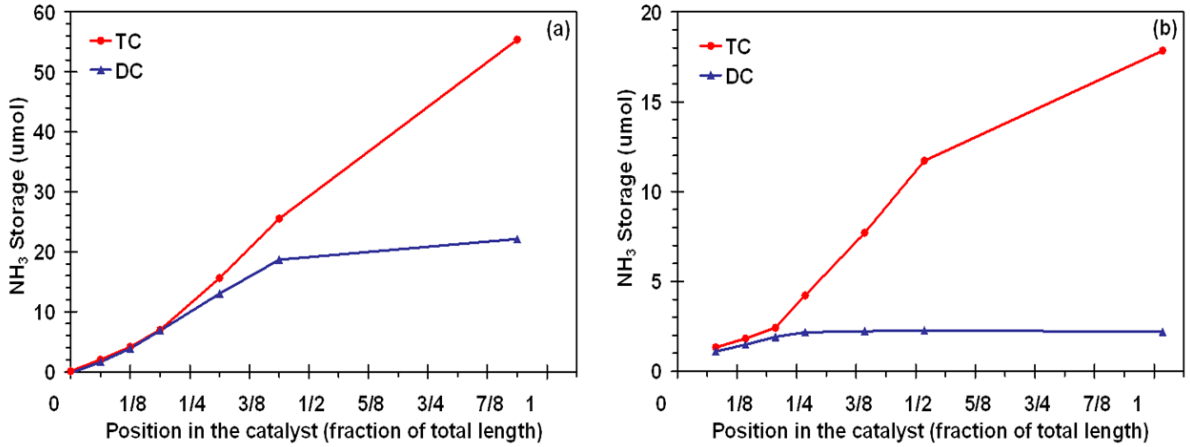

Figure 30: Storage capacity distributions at (a) 200°C and (b) 325°C.

UC is the additional storage capacity observed in step 3 after performing SCR. In the SCR zone, DC is equal to TC because all storage sites can be filled during step 2 as long as NH_3 is not fully consumed. As a result, there are no available sites for NH_3 to store in that section of the catalyst when step 3 starts (NO is turned off) and UC is, therefore, zero in the SCR zone. However, UC increases rapidly in the post-SCR zone and is responsible for a major part of the total capacity of the whole catalyst. Figure 31 shows the ammonia concentration for different locations in step 3 of the protocol at 325°C. It can be seen that the ammonia curves for the first three locations are similar and present a small residual apparent storage. It should be mentioned that some of this

storage is likely due to slow ammonia response in the system. Thus, the occurrence of no or only minor UC storage in step 3 is consistent with the other measurements, which yielded similar DC and TC in the SCR zone. As we move the capillary further down in the catalyst, the time to reach saturation increases reflecting the increase of NH_3 storage.

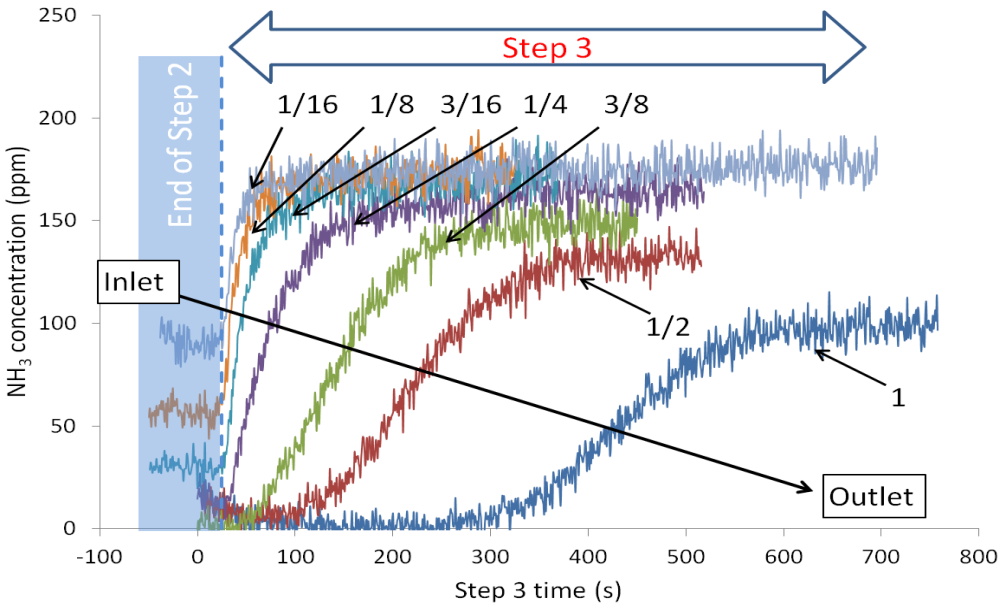

Figure 31: NH_3 concentration profiles in step 3 at 325°C at 1/16, 1/8, 3/16, 1/4, 3/8, 1/2 and 1L locations.

6. Conclusions and outlook

Within the framework of reducing vehicle emissions, two studies were conducted. The investigation of the ageing of a platinum-based DOC provided insight into the specific impact of temperature and reactive atmosphere on Pt sintering as well as the activity toward NO oxidation. The latter reaction was found to be faster on larger particles, i.e. on thermally aged catalysts, which yielded higher conversion. Impact of increasing the ageing temperature was to decrease the Pt dispersion down to a low limit. As a consequence, the catalytic activity increased with ageing. The nature of ageing atmosphere had a significant influence on the rate of sintering and NO conversion upon ageing. Thus, oxygen was found to promote the activity after ageing at low temperature and led to a lower final dispersion than was obtained in Ar. A slight deactivation of catalysts aged in the presence of O_2 after high temperature ageing was noted. This feature was not observed on the other samples which presented an increase of activity after every ageing step. SO_2 showed an interesting ability to enhance sintering at low ageing temperature, as well as improving the activity of aged catalysts. The disparity of activities for similar dispersion emphasized the important role of the ageing atmosphere in further catalytic performance. The reasons of these improvements by the ageing atmosphere are still unclear and it would be beneficial to conduct more characterization of the catalysts.

The second study was to investigate NO_x reduction by ammonia SCR on a Cu-Beta zeolite catalyst. Many reactions may occur and compete with the SCR reaction when using an inlet flow consisting of NO, NH_3 and O_2. Moreover, zeolites provide a large surface area and many acidic sites where NH_3 can readily store. The spatial distribution of the SCR reaction, as well as NO and NH_3 oxidation, was resolved using SpaciMS developed in the Fuel, Engines and Emissions Research Center (FEERC) at ORNL together with Cummins Inc. The consumption of NO and NH_3, as well as the formation of reaction products like N_2 and N_2O, were monitored along the catalyst. Thus, the activity and selectivity of the catalyst were evaluated. Our results showed that there exists a zone where SCR occurs until NH_3 is fully consumed. Within that zone, called SCR zone, all NH_3 storage sites are filled during SCR operation. When the storage is completed, SCR reaction reaches steady state with a 1:1 stoichiometry as predicted by the standard SCR equation. At 200 and 325°C, the storage capacities followed the same pattern in which the dynamic capacity is similar to the total capacity within the SCR zone and remains constant, while total capacity increases linearly due to the parallel increase of unused capacity. At 400°C, only minor amounts of ammonia were stored. It would be interesting to conduct spatially resolved experiments of the storage capacity and activity after hydrothermal ageing.

Acknowledgments

The Swedish Foundation for Strategic Research is gratefully acknowledged for funding this project. This work was performed at the Competence Centre for Catalysis (KCK), Chalmers University of Technology. KCK is financially supported by Chalmers University of Technology, the Swedish Energy Agency and the member companies: AB Volvo, Volvo Car Corporation, Scania CV AB, Saab Automobile Powertrain AB, Haldor Topsoe A/S and ECAPS AB.

I would like to thank Professor Bengt Andersson and Professor Louise Olsson for giving me the opportunity to do my PhD at Chalmers.

Louise, again, for being such a great supervisor, for fixing all the incredible problems I faced, for her support and for the good work we did.

My Tennessean buddies Bill Partridge and Jae-Soon Choi for the awesome time I had in the Volunteer State as well as the good teamwork we pulled off.

Finally, I thank my family and friends for their unfailing support.

7. References

[1] S.G. Masters, D. Chadwick, Selective reduction of nitric oxide by methanol and dimethyl ether over promoted alumina catalysts in excess oxygen, Applied Catalysis B: Environmental, 23 (1999) 235-246.
[2] F.C. Meunier, J.P. Breen, V. Zuzaniuk, M. Olsson, J.R.H. Ross, Mechanistic aspects of the selective reduction of NO by propene over alumina and silver-alumina catalysts, Journal of Catalysis, 187 (1999) 493-505.
[3] M. Devadas, O. Kröcher, M. Elsener, A. Wokaun, N. Söger, M. Pfeifer, Y. Demel, L. Mussmann, Influence of NO_2 on the selective catalytic reduction of NO with ammonia over Fe-ZSM5, Applied Catalysis B: Environmental, 67 (2006) 187-196.
[4] M. Koebel, G. Madia, M. Elsener, Selective catalytic reduction of NO and NO_2 at low temperatures, Catalysis Today, 73 (2002) 239-247.
[5] I. Nova, C. Ciardelli, E. Tronconi, D. Chatterjee, B. Bandl-Konrad, NH_3-NO/NO_2 chemistry over V-based catalysts and its role in the mechanism of the Fast SCR reaction, Catalysis Today, 114 (2006) 3-12.
[6] M. Koebel, M. Elsener, M. Kleemann, Urea-SCR: a promising technique to reduce NO_x emissions from automotive diesel engines, Catalysis Today, 59 (2000) 335-345.
[7] J.-Y. Luo, X. Hou, P. Wijayakoon, S.J. Schmieg, W. Li, W.S. Epling, Spatially resolving SCR reactions over a Fe/zeolite catalyst, Applied Catalysis B: Environmental, 102 (2011) 110-119.
[8] A. Grossale, I. Nova, E. Tronconi, D. Chatterjee, M. Weibel, The chemistry of the NO/NO_2-NH_3 "fast" SCR reaction over Fe-ZSM5 investigated by transient reaction analysis, Journal of Catalysis, 256 (2008) 312-322.
[9] T. Komatsu, M. Nunokawa, I.S. Moon, T. Takahara, S. Namba, T. Yashima, Kinetic Studies of Reduction of Nitric Oxide with Ammonia on Cu2+-Exchanged Zeolites, Journal of Catalysis, 148 (1994) 427-437.
[10] K. Rahkamaa-Tolonen, T. Maunula, M. Lomma, M. Huuhtanen, R.L. Keiski, The effect of NO_2 on the activity of fresh and aged zeolite catalysts in the NH_3-SCR reaction, Catalysis Today, 100 (2005) 217-222.
[11] H. Sjövall, L. Olsson, E. Fridell, R.J. Blint, Selective catalytic reduction of NO_x with NH_3 over Cu-ZSM-5-The effect of changing the gas composition, Applied Catalysis B: Environmental, 64 (2006) 180-188.
[12] J. Després, M. Elsener, M. Koebel, O. Kröcher, B. Schnyder, A. Wokaun, Catalytic oxidation of nitrogen monoxide over Pt/SiO_2, Applied Catalysis B: Environmental, 50 (2004) 73-82.
[13] M.F. Irfan, J.H. Goo, S.D. Kim, S.C. Hong, Effect of CO on NO oxidation over platinum based catalysts for hybrid fast SCR process, Chemosphere, 66 (2007) 54-59.
[14] L. Olsson, B. Westerberg, H. Persson, E. Fridell, M. Skoglundh, B. Andersson, A Kinetic Study of Oxygen Adsorption/Desorption and NO Oxidation over Pt/Al_2O_3 Catalysts, Journal of Physical Chemistry B, 103 (1999) 10433-10439.
[15] M. Crocoll, S. Kureti, W. Weisweiler, Mean field modeling of NO oxidation over Pt/Al_2O_3 catalyst under oxygen-rich conditions, Journal of Catalysis, 229 (2005) 480-489.
[16] S.S. Mulla, N. Chen, W.N. Delgass, W.S. Epling, F.H. Ribeiro, NO_2 inhibits the catalytic reaction of NO and O_2 over Pt, Catal Lett, 100 (2005) 267-270.
[17] P.J. Schmitz, R.J. Kudla, A.R. Drews, A.E. Chen, C.K. Lowe-Ma, R.W. McCabe, W.F. Schneider, C.T. Goralski Jr, NO oxidation over supported Pt: Impact of precursor, support, loading, and processing conditions evaluated via high throughput experimentation, Applied Catalysis B: Environmental, 67 (2006) 246-256.
[18] A.D. Smeltz, R.B. Getman, W.F. Schneider, F.H. Ribeiro, Coupled theoretical and experimental analysis of surface coverage effects in Pt-catalyzed NO and O_2 reaction to NO_2 on Pt(1 1 1), Catalysis Today, 136 (2008) 84-92.

[19] D. Bhatia, R.W. McCabe, M.P. Harold, V. Balakotaiah, Experimental and kinetic study of NO oxidation on model Pt catalysts, Journal of Catalysis, 266 (2009) 106-119.
[20] S.S. Mulla, N. Chen, L. Cumaranatunge, G.E. Blau, D.Y. Zemlyanov, W.N. Delgass, W.S. Epling, F.H. Ribeiro, Reaction of NO and O_2 to NO_2 on Pt: Kinetics and catalyst deactivation, Journal of Catalysis, 241 (2006) 389-399.
[21] W. Haifeng, G. Yanglong, L. Guanzhong, P. Hu, An understanding and implications of the coverage of surface free sites in heterogeneous catalysis, Journal of Chemical Physics, 130 (2009) 224701 (224706 pp.).
[22] E. Xue, K. Seshan, J.R.H. Ross, Roles of supports, Pt loading and Pt dispersion in the oxidation of NO to NO_2 and of SO_2 to SO_3, Applied Catalysis B: Environmental, 11 (1996) 65-79.
[23] S. Benard, L. Retailleau, F. Gaillard, P. Vernoux, A. Giroir-Fendler, Supported platinum catalysts for nitrogen oxide sensors, Applied Catalysis B: Environmental, 55 (2005) 11-21.
[24] L. Olsson, E. Fridell, The Influence of Pt Oxide Formation and Pt Dispersion on the Reactions $NO_2 \leftrightarrow NO+1/2\ O_2$ over Pt/Al_2O_3 and $Pt/BaO/Al_2O_3$, Journal of Catalysis, 210 (2002) 340-353.
[25] R.D. Clayton, M.P. Harold, V. Balakotaiah, C.Z. Wan, Pt dispersion effects during NOx storage and reduction on $Pt/BaO/Al_2O_3$ catalysts, Applied Catalysis B: Environmental, 90 (2009) 662-676.
[26] J. Yang, V. Tschamber, D. Habermacher, F. Garin, P. Gilot, Effect of sintering on the catalytic activity of a Pt based catalyst for CO oxidation: Experiments and modeling, Applied Catalysis B: Environmental, 83 (2008) 229-239.
[27] Y. Yazawa, N. Kagi, S.I. Komai, A. Satsuma, Y. Murakami, T. Hattori, Kinetic study of support effect in the propane combustion over platinum catalyst, Catal Lett, 72 (2001) 157-160.
[28] S. Ovesson, B.I. Lundqvist, W.F. Schneider, A. Bogicevic, NO oxidation properties of Pt(111) revealed by ab initio kinetic simulations, Physical Review B (Condensed Matter and Materials Physics), 71 (2005) 115406-115401.
[29] K. Mudiyanselage, Y. Cheol-Woo, J. Szanyi, Oxygen coverage dependence of NO oxidation on Pt(111), Journal of Physical Chemistry C, 113 (2009) 5766-5776.
[30] H.F. Wang, Y.L. Guo, G. Lu, P. Hu, NO oxidation on platinum group metals oxides: First principle calculations combined with microkinetic analysis, Journal of Physical Chemistry C, 113 (2009) 18746-18752.
[31] R.W. McCabe, C. Wong, H.S. Woo, The passivating oxidation of platinum, Journal of Catalysis, 114 (1988) 354-367.
[32] Y.F. Chu, E. Ruckenstein, On the sintering of platinum on alumina model catalyst, Journal of Catalysis, 55 (1978) 281-298.
[33] T. Tanabe, Y. Nagai, K. Dohmae, H. Sobukawa, H. Shinjoh, Sintering and redispersion behavior of Pt on Pt/MgO, Journal of Catalysis, 257 (2008) 117-124.
[34] A. Monzón, T.F. Garetto, A. Borgna, Sintering and redispersion of $Pt/\gamma\text{-}Al_2O_3$ catalysts: A kinetic model, Applied Catalysis A: General, 248 (2003) 279-289.
[35] H. Glassl, R. Kramer, K. Hayek, Electron microscopy of Pt/Al_2O_3 model catalysts. II. Sintering in atmospheres of H_2, O_2 and Ar, Journal of Catalysis, 68 (1981) 388-396.
[36] P.C. Flynn, S.E. Wanke, A model of supported metal catalyst sintering : I. Development of model, Journal of Catalysis, 34 (1974) 390-399.
[37] P.C. Flynn, S.E. Wanke, A model of supported metal catalyst sintering : II. Application of model, Journal of Catalysis, 34 (1974) 400-410.
[38] P.C. Flynn, S.E. Wanke, Experimental studies of sintering of supported platinum catalysts, Journal of Catalysis, 37 (1975) 432-448.
[39] T.J. Lee, Y.G. Kim, Redispersion of supported platinum catalysts, Journal of Catalysis, 90 (1984) 279-291.
[40] B. Pulvermacher, E. Ruckenstein, Identification of the rate determining step in aging of supported metals, Journal of Catalysis, 35 (1974) 115-139.
[41] E. Ruckenstein, Role of wetting in sintering and redispersion of supported metal crystallites, Journal of Crystal Growth, 47 666-670.

[42] E. Ruckenstein, M.L. Malhotra, Splitting of platinum crystallites supported on thin, nonporous alumina films, Journal of Catalysis, 41 (1976) 303-311.
[43] P. Loof, B. Stenbom, H. Norden, B. Kasemo, Rapid Sintering in NO of Nanometer-Sized Pt Particles on γ-Al_2O_3 Observed by CO Temperature-Programmed Desorption and Transmission Electron Microscopy, Journal of Catalysis, 144 (1993) 60-76.
[44] N. Kamiuchi, K. Taguchi, T. Matsui, R. Kikuchi, K. Eguchi, Sintering and redispersion of platinum catalysts supported on tin oxide, Applied Catalysis B: Environmental, 89 (2009) 65-72.
[45] Y. Murakami, S. Komai, T. Hattori, Accelerated Sintering of Pt Catalysts in Reaction Atmosphere for Rapid Estimation of Catalyst Life, in, 1991, pp. 645-652.
[46] A. Winkler, D. Ferri, M. Aguirre, The influence of chemical and thermal aging on the catalytic activity of a monolithic diesel oxidation catalyst, Applied Catalysis B: Environmental, 93 (2009) 177-184.
[47] R.M.J. Fiedorow, S.E. Wanke, The sintering of supported metal catalysts. I. Redispersion of supported platinum in oxygen, Journal of Catalysis, 43 (1976) 34-42.
[48] M.J. D'Aniello Jr, D.R. Monroe, C.J. Carr, M.H. Krueger, The redispersion of sintered Pt, Rh, and Pt Rh catalysts, Journal of Catalysis, 109 (1988) 407-422.
[49] J.M. Rickard, L. Genovese, A. Moata, S. Nitsche, Redispersion of platinum on Pt/Al_2O_3 model catalyst in oxygen studied by transmission electron microscopy, Journal of Catalysis, 121 (1990) 141-152.
[50] I. Sushumna, E. Ruckenstein, Redispersion of Pt/alumina via film formation, Journal of Catalysis, 108 (1987) 77-96.
[51] K. Foger, H. Jaeger, Redispersion of Pt/zeolite catalysts with chlorine, Applied Catalysis, 56 (1989) 137-147.
[52] E. Ruckenstein, X.D. Hu, Mechanism of redispersion of supported metal catalysts in oxidative atmospheres, Langmuir, 1 (1985) 756-760.
[53] E. Ruckenstein, B. Pulvermacher, Growth kinetics and the size distributions of supported metal crystallites, Journal of Catalysis, 29 (1973) 224-245.
[54] J.C. Summers, Reaction of sulfur oxides with alumina and platinum/alumina, Environmental Science and Technology, 13 (1979) 321-325.
[55] L. Limousy, H. Mahzoul, J.F. Brilhac, P. Gilot, F. Garin, G. Maire, SO_2 sorption on fresh and aged SO_x traps, Applied Catalysis B: Environmental, 42 (2003) 237-249.
[56] P. Engström, A. Amberntsson, M. Skoglundh, E. Fridell, G. Smedler, Sulphur dioxide interaction with NO_x storage catalysts, Applied Catalysis B: Environmental, 22 (1999) L241-L248.
[57] J. Andersson, M. Antonsson, L. Eurenius, E. Olsson, M. Skoglundh, Deactivation of diesel oxidation catalysts: Vehicle- and synthetic aging correlations, Applied Catalysis B: Environmental, 72 (2007) 71-81.
[58] R. Giles, N.W. Cant, M. Kögel, T. Turek, D.L. Trimm, The effect of SO_2 on the oxidation of NO over Fe-MFI and Fe-ferrierite catalysts made by solid-state ion exchange, Applied Catalysis B: Environmental, 25 (2000) L75-L81.
[59] L. Olsson, H. Karlsson, The beneficial effect of SO_2 on platinum migration and NO oxidation over Pt containing monolith catalysts, Catalysis Today, 147 (2009) S290-S294.
[60] J.H. Pazmiño, J.T. Miller, S.S. Mulla, W. Nicholas Delgass, F.H. Ribeiro, Kinetic studies of the stability of Pt for NO oxidation: Effect of sulfur and long-term aging, Journal of Catalysis.
[61] A.F. Lee, K. Wilson, R.M. Lambert, C.P. Hubbard, R.G. Hurley, R.W. McCabe, H.S. Gandhi, The Origin of SO_2 Promotion of Propane Oxidation over Pt/Al_2O_3 Catalysts, Journal of Catalysis, 184 (1999) 491-498.
[62] T.N. Angelidis, N. Kruse, Promotional effect of SO_2 on the selective catalytic reduction of NOx with propane/propene over Ag/γ-Al_2O_3, Applied Catalysis B: Environmental, 34 (2001) 201-212.
[63] K. Foger, J.R. Anderson, Temperature programmed desorption of carbon monoxide adsorbed on supported platinum catalysts, Applications of Surface Science, 2 (1979) 335-351.

[64] L. Olsson, M. Abul-Milh, H. Karlsson, E. Jobson, P. Thormählen, A. Hinz, The effect of a changing lean gas composition on the ability of NO_2 formation and NO_x reduction over supported Pt catalysts, Topics in Catalysis, 30-31 (2004) 85-90.
[65] I. Guo, T.T. Yu, S.E. Wanke, Changes in Pt crystallite sizes as a result of treating Pt/Al_2O_3 catalysts in different atmospheres, in, 1988, pp. 21-32.
[66] K. Foger, Catalysis : Science and technology, Springer, Verlag Berlin Heidelberg New York Tokyo, 1984.
[67] J.S. Choi, W.P. Partridge, C.S. Daw, Spatially resolved in situ measurements of transient species breakthrough during cyclic, low-temperature regeneration of a monolithic $Pt/K/Al_2O_3$ NOx storage-reduction catalyst, Applied Catalysis A: General, 293 (2005) 24-40.
[68] J.S. Choi, W.P. Partridge, C.S. Daw, Sulfur impact on NO_x storage, oxygen storage, and ammonia breakthrough during cyclic lean/rich operation of a commercial lean NO_x trap, Applied Catalysis B: Environmental, 77 (2007) 145-156.
[69] J.-S. Choi, W.P. Partridge, W.S. Epling, N.W. Currier, T.M. Yonushonis, Intra-channel evolution of carbon monoxide and its implication on the regeneration of a monolithic $Pt/K/Al_2O_3$ NO_x storage-reduction catalyst, Catalysis Today, 114 (2006) 102-111.
[70] W.P. Partridge, J.S. Choi, NH_3 formation and utilization in regeneration of $Pt/Ba/Al_2O_3$ NO_x storage-reduction catalyst with H_2, Applied Catalysis B: Environmental, 91 (2009) 144-151.
[71] W.P. Partridge, T.J. Toops, J.B. Green, T.R. Armstrong, Intra-fuel cell stack measurements of transient concentration distributions, Journal of Power Sources, 160 (2006) 454-461.
[72] J. Sá, D.L.A. Fernandes, F. Aiouache, A. Goguet, C. Hardacre, D. Lundie, W. Naeem, W.P. Partridge, C. Stere, SpaciMS: Spatial and temporal operando resolution of reactions within catalytic monoliths, Analyst, 135 (2010) 2260-2272.
[73] K. Irani, W.S. Epling, R. Blint, Spatial resolution of reactant species consumption in diesel oxidation catalysts, Topics in Catalysis, 52 (2009) 1856-1859.
[74] A. Russell, W.S. Epling, H. Hess, H.Y. Chen, C. Henry, N. Currier, A. Yezerets, Spatially-resolved temperature and gas species changes in a lean-burn engine emissions control catalyst, Industrial and Engineering Chemistry Research, 49 (2010) 10311-10322.
[75] O. Shakir, A. Yezerets, N.W. Currier, W.S. Epling, Spatially resolving concentration and temperature gradients during the oxidation of propylene on Pt/Al_2O_3, Applied Catalysis A: General, 365 (2009) 301-308.
[76] K. Kamasamudram, N.W. Currier, X. Chen, A. Yezerets, Overview of the practically important behaviors of zeolite-based urea-SCR catalysts, using compact experimental protocol, Catalysis Today, 151 (2010) 212-222.
[77] C.R. Apesteguia, T.F. Garetto, A. Borgna, On the sulfur-aided metal-support interaction in Pt/Al_2O_3-Cl catalysts, Journal of Catalysis, 106 (1987) 73-84.
[78] O. Kröcher, M. Widmer, M. Elsener, D. Rothe, Adsorption and desorption of SO_x on diesel oxidation catalysts, Industrial and Engineering Chemistry Research, 48 (2009) 9847-9857.
[79] L. Kylhammar, P.A. Carlsson, H.H. Ingelsten, H. Grönbeck, M. Skoglundh, Regenerable ceria-based SO_x traps for sulfur removal in lean exhausts, Applied Catalysis B: Environmental, 84 (2008) 268-276.
[80] R. Streber, C. Papp, M.P.A. Lorenz, O. Höfert, E. Darlatt, A. Bayer, R. Denecke, H.P. Steinrück, SO_2 adsorption and thermal evolution on clean and oxygen precovered Pt(111), Chemical Physics Letters, 494 (2010) 188-192.
[81] P. Zebisch, M. Stichler, P. Trischberger, M. Weinelt, H.P. Steinrück, Adsorption and thermal evolution of SO_2 on the Pt(110) surface, Surface Science, 371 (1997) 235-244.
[82] L. Gang, J. Van Grondelle, B.G. Anderson, R.A. Van Santen, Selective low temperature NH_3 oxidation to N_2 on copper-based catalysts, Journal of Catalysis, 186 (1999) 100-109.
[83] G. Delahay, B. Coq, S. Kieger, B. Neveu, The origin of N_2O formation in the selective catalytic reduction of NO_x by NH_3 in O_2 rich atmosphere on Cu-faujasite catalysts, Catalysis Today, 54 (1999) 431-438.